

Galaxy Evolution, Deep Galaxy Counts and the Near-IR Cosmic Infrared Background.

R. Jimenez¹, A. Kashlinsky^{2,3,4}

¹Institute for Astronomy, University of Edinburgh, Royal Observatory Edinburgh, Blackford Hill, Edinburgh EH9 3HJ, UK

²Raytheon STX, Code 685, NASA Goddard Space Flight Center, Greenbelt, MD 20771

³NORDITA, Blegdamsvej 17, DK-2100 Copenhagen, Denmark

⁴Theoretical Astrophysics Center, Juliane Maries Vej 30, DK-2100 Copenhagen, Denmark

Received _____; accepted _____

ABSTRACT

Accurate synthetic models of stellar populations are constructed and used in evolutionary models of stellar populations in forming galaxies. Following their formation, the late type galaxies are assumed to follow the Schmidt law for star formation, while early type galaxies are normalized to the present-day fundamental plane relations assumed to mimic the metallicity variations along their luminosity sequence. The stars in disks of galaxies are distributed with the Scalo IMF and in spheroids with the Salpeter IMF. We show that these assumptions reproduce extremely well the recent observations for the evolution of the rate of star formation with redshift. We then compute predictions of these models for the observational data at early epochs for various cosmological parameters Ω , Ω_Λ and H_0 . We find good match to the metallicity data from the damped L_α systems and the evolution of the luminosity density out to $z \simeq 1$. Likewise, our models provide good fits for low values of Ω to the deep number counts of galaxies in all bands where data is available; this is done without assuming existence of extra populations of galaxies at high z . Our models also match the data on the redshift distribution of galaxy counts in B and K bands. We compute the predicted mean levels and angular distribution of the cosmic infrared background produced from the early evolution of galaxies. The predicted fluxes and fluctuations are still below the current observational limits, but not by a large factor. Finally, we find that the recent detection of the diffuse extragalactic light in the visible bands requires for our models high redshift of galaxy formation, $z_f \geq (3-4)$; otherwise the produced flux of the extragalactic light at optical bands exceeds the current observational limits.

Subject headings: Cosmology: Theory – Galaxies: Evolution – Diffuse Radiation – Large Scale Structure of the Universe

1. Introduction

The epoch and process of galaxy formation are still a matter of considerable debate despite substantial recent observational and theoretical progress. On the observational side, it is becoming increasingly clear that galaxies must have formed early on in the evolution of the Universe with the farthest galaxies known to date having redshifts of 5 and beyond (Franx et al. 1997; Spinrad et al. 98, in preparation). Similarly, such high redshift of formation of the first stellar populations in galaxies is indicated by the existence of galaxies at moderately high redshifts, $z \sim 1.5$, but which contain old stellar populations of about 3.5-4 Gyr (Dunlop et al. 1996, Dunlop 1998). On theoretical front, the existence of galaxies at these redshifts coupled with the data on large-scale galaxy distribution at the present day allow one to reconstruct the spectrum of the pregalactic density field (Kashlinsky 1998), which however is not in good agreement with popular cold-dark-matter models based on inflationary paradigm.

Other data do not involve record numbers for redshifts of still only a handful of galaxies, but are just as important. Such data come from the deep galaxy counts probing galaxies in various spectroscopic bands, from blue to near-infrared. It too constrains both galaxy evolution and global cosmological parameters. The data on galaxy counts are now coupled with the newly obtained measurements of the luminosity density produced by galaxies in UV, V and J (1.25 micron) bands at $z \leq 1$ from Lilly et al. (1996) and the new data on the evolution of cosmic abundances out to high redshift (Pettini et al. 1997). Furthermore, there are now independent measurements of the star formation rate out to high redshifts (Madau et al. 1996); these show that star formation increases out to $z \simeq 2$ with a possible peak at $z \sim (2-3)$.

All such data allow one to reconstruct the early evolution of galaxies and stellar populations in the Universe thereby providing an important test of galaxy formation processes and the underlying cosmology. In computing such evolution one must necessarily normalize galaxy populations to the present-day data, e.g. galaxy luminosity function in the relevant bands and the morphological mixes. The present-day luminosity function of galaxies has now been measured accurately in B (Loveday et al. 1992) and K bands (Gardner et al. 1997) and the morphological mixes at the present epoch are also well determined (Marzke et al. 1994). With the input of the Initial Mass Function (IMF) for the various galaxy types and specifying their star formation history, one can uniquely compute individual galaxy populations out to very early times.

Individual galaxy observations, however, provide only a limited amount of information on the overall evolution of galaxies and the Universe and are expensive in terms of time involved and area covered. On the other hand, diffuse background radiation fields left over from galaxy formation and evolution

contain cumulative information about the entire evolution of the Universe including radiation from objects inaccessible to telescopic studies. Cosmic Infrared Background (CIB) occupies a unique space among the various diffuse background produced by galaxies. The reason is that the bulk of any stellar light emitted at early times will reach the observer shifted into the near to far-IR. CIB thus probes early galaxy formation and evolution and contains cumulative information on the history of the Universe over redshifts between the epoch of the last scattering surface, probed by the microwave background, and $z \sim 0$, probed by the surveys in visible bands.

On the observational side, no detection of the putative CIB has been made at wavelengths below $100 \mu\text{m}$. At wavelengths beyond $150 \mu\text{m}$ there are claims of possible detections from the COBE DIRBE (Hauser et al. 1998; Schlegel, Finkbeiner & Davis 1998) and FIRAS (Puget et al. 1996) maps. In the near-IR, arguments based on chemical evolution predict levels of CIB around $\sim 10 \text{ nW m}^{-2} \text{ sr}^{-1}$ (Stecker, Puget & Fazio 1977). The Galactic and zodiacal foregrounds are very bright at these wavelengths so it is very difficult to reach such limits directly as analysis of d.c. levels of DIRBE maps indicates (Hauser et al. 1998). On the other hand, comparable levels can be reached with fluctuations analysis of the near-IR CIB (Kashlinsky, Mather & Odenwald 1996; Kashlinsky et al. 1996; Kashlinsky, Mather & Odenwald, 1998 in preparation) and there is hope of reaching the CIB levels directly with this method applied to other surveys. In optical bands, Vogeley (1997) has derived strong limits of the diffuse background at R and B from the fluctuations analysis of the Hubble Deep Field.

At the same time, significant progress has been made in the last few years in theoretical understanding of evolution of stellar populations as new opacities have become available (OPAL 95 and Alexander, 1998 private communication) for computing stellar interiors from the contracting Hayashi track to the white dwarf (or carbon ignition) phase. Photospheric modeling has reached high accuracy with theoretical models resembling very closely observed spectra from individual stars (Jimenez et al. 1998). Furthermore, the new Hipparcos data allow for a much better calibration of the isochrones at the main-sequence (see Jimenez & Flynn 1997 for more details) in conjunction with the classical calibration to the Sun. This then allows to construct self-consistent stellar population models that are properly calibrated to the Sun and to the Hipparcos data and therefore are more reliable than previous models. Also new stellar yields are now available (see section 4.1) and chemical evolution can be done more accurately.

It is therefore, imperative and timely to explore the limits and predictions that models of stellar evolution make in light of the new data, such as chemical contents at early epochs, the evolution of star

formation and luminosity density with time, as well as the spatial and other properties of the near-IR CIB and optical diffuse backgrounds.

The outline of this paper is as follows: in Section 2 we discuss the cosmological context for the calculations we present in this paper. Section 3 discusses the stellar populations models we use for galaxy evolution. Modeling evolution of different galaxy types which at the same time is normalized to the data on modern galaxies and the redshift of galaxy formation is presented in Section 4. In Section 5 we compare our results to the data: we reproduce the evolution of chemical abundances at high z , the data on the luminosity density in UV, B and J bands from Lilly et al. (1996); the available data on deep galaxy counts in the various bands; and in Section 5.4 compute properties of the near-IR CIB for the models that successfully reproduce the above data. Our conclusions are summarized in Section 6.

2. Cosmological context

Galaxy evolution models are now constrained by the recent data containing cumulative information on galaxy evolution at early epochs. In this paper we concentrate on and aim to construct galaxy evolutionary models to constrain the following: 1) the evolution of the total emissivity in the various bands with redshift. This data has been recently obtained by Lilly et al. (1996) from the CFRS faint galaxy survey in three bands (UV, B and J) out to $z \leq 1$. 2) The data on deep galaxy counts in different photometric bands. 3) The current limits on the DC levels and fluctuations in the CIB and diffuse background light at optical wavelengths. While the current data on the near-IR CIB has not yet resulted in firm detections, the latest upper limits come very close to the cosmologically interesting levels. On the other hand, in optical bands there is now positive detection of the diffuse background light. We therefore aim to accurately compute the expected levels of the near-IR CIB and its structure that can be uncovered in future searches.

We define with $L_\lambda(\lambda; z)$ the luminosity per wavelength interval $d\lambda$ centered on wavelength λ in the rest-frame of the galaxy located at redshift z . The emissivity per unit wavelength produced by galaxies at redshift z and observed today through a filter with band-width $d\lambda$ centered at wavelength λ is:

$$\epsilon_\lambda(z) = (1+z)^{-1} \sum_i \int L_{\lambda,i} \left(\frac{\lambda}{1+z}; z \right) dN \quad (1)$$

where dN is the comoving number density of such galaxies which is given by the luminosity function of galaxies at z . If the number of galaxies is fixed since their formation then the latter is given by the present-day blue (or red) luminosity of galaxies, i.e. $dN = \Phi_0(L_B) dL_B$. In our calculations we compute the

emissivity after normalizing to the data on the present-day galaxy luminosity function in both blue (B) and red (K) bands. The sum in eq. (1) is taken over all galaxy types. The emissivity per unit frequency is $\nu\epsilon_\nu(z) = (1+z)^2\lambda\epsilon_\lambda(z)$.

Another set of quantities that depend on galaxy evolutionary history in a variety of bands, but in a different way than the emissivity, are deep counts of galaxies. The data is now available in four bands: B, R, I, K (e.g. see Koo & Kron (1992) for review). The number of galaxies, \mathcal{L} , per unit solid angle observed through the aperture in the rest frame band j in the apparent magnitude interval $[m; m+dm]$ is given per dz by:

$$\frac{d\mathcal{N}_j}{dz} = \frac{dV}{dz} dN(m_j; m_j + dm_j) \quad (2)$$

where the comoving volume occupied by unit solid angle in the redshift interval dz is $dV/dz = (1+z)x^2(z)cdt/dz$. The cosmic time-redshift relation depends on the global cosmological parameters via:

$$H_0 \frac{dt}{dz} = \frac{1}{(1+z)^2 \sqrt{1 + \Omega z + \Omega_\Lambda[(1+z)^{-2} - 1]}} \quad (3)$$

The last two quantities, which reflect still another dependence on cosmic epoch and evolution, relate to the levels of the CIB produced by such evolving galaxy populations: the DC (mean) levels of the CIB and the levels of fluctuations in its angular distribution. The flux received per unit wavelength in band λ from each galaxy with luminosity L_λ at redshift z is $\frac{L_\lambda(\lambda/(1+z); z)}{4\pi x^2(1+z)^3}$. Multiplying this with dN , then integrating over all the luminosities, summing over all the galaxy types and multiplying by dV/dz gives the flux produced per redshift interval dz :

$$\frac{dF}{dz} = \frac{R_H}{4\pi} \frac{1}{(1+z)^2} \frac{d(H_0 t)}{dz} [\lambda\epsilon_\lambda(z)] = \frac{R_H}{4\pi} \frac{d(H_0 t)}{dz} [\nu\epsilon_\nu(z)] \quad (4)$$

where $F = \lambda I_\lambda = \nu I_\nu$ is the total CIB flux in band λ received from evolving galaxies.

An additional measure of the CIB produced by galaxies and thereby of the early evolution of stellar populations is its spatial structure. Until recently, no attempts have been made to measure CIB fluctuations although some theoretical calculations existed in the mid to far-IR (Wang 1991). Recently, observational progress has been made from studying COBE DIRBE all-sky maps (Kashlinsky, Mather & Odenwald 1996; Kashlinsky et al. 1996) resulting in interesting upper limits, but so far no firm detections. Since galaxies producing the CIB are clustered, their clustering pattern should in turn be reflected in the structure of the CIB. A convenient way to characterize the CIB fluctuations, $\delta F(\boldsymbol{\theta}) \equiv F(\boldsymbol{\theta}) - \langle F \rangle$, is via its correlation function, $C(\theta) \equiv \langle \delta F(\mathbf{x} + \boldsymbol{\theta}) \delta F(\mathbf{x}) \rangle$. Its two-dimensional Fourier transform is the power

spectrum $P(q) = \langle |\delta F_q|^2 \rangle$, where $\delta F(\boldsymbol{\theta}) = (2\pi)^{-2} \int \delta F_q \exp(-i\boldsymbol{q} \cdot \boldsymbol{\theta}) d^2 \boldsymbol{q}$. The rms fluctuation in the the CIB flux on scale $\theta \simeq \pi/q$ is $\delta F_{\text{rms}} \simeq \sqrt{q^2 P_2(q)/2\pi}$.

The two-dimensional angular correlation of the CIB is related to the underlying three-dimensional galaxy correlation function and the rate of flux production, dF/dz , via the projection equation otherwise known as the Limber equation (Peebles 1980). One can show via the Limber equation that the angular power spectrum of the CIB, $P_2(q)$, is related to that of the present-day galaxy clustering, $P_3(k)$, via (Kashlinsky, Mather & Odenwald 1998, in preparation):

$$\frac{d}{dz} [q^2 P_2(q)] = \left(\frac{dF}{dz} \right)^2 \frac{\Psi^2(z)}{H_0 \frac{dt}{dz}} \Delta^2 \left(\frac{q(1+z)}{x(z)} \right) \quad (5)$$

where $\Delta(k) = \sqrt{R_H^{-1} k^2 P_3(k)}$, $P_3(k)$ is the three-dimensional power spectrum of the present-day galaxy distribution, or the three-dimensional Fourier transform of the two-point galaxy correlation function, and $\Psi(z)$ is the growth factor accounting for the evolution (growth) of the clustering pattern with time. The latter can be scale dependent since non-linear and linear scales may evolve differently. The quantity $\Delta(k)$ is essentially an order-of-magnitude fluctuation in galaxies over the line-of-sight cylinder of length R_H and diameter k^{-1} . Thus the net fluctuations in the CIB reflect a different dependence on the rate of CIB production than the mean (DC) flux in eq.(4), and are also weighed in the integrand with the quantity Δ^2 containing the galaxy clustering power spectrum. (The correlation function, or power spectrum, being the two-point process, depends on the integral over the second power of dF/dz). Therefore measuring CIB fluctuations in conjunction with the DC levels will provide important information on the dF/dz dependence in addition to the total flux levels.

The set of the quantities given by equations (1)-(5) in this Section produces numbers that have very different dependences (integral and differential) on the early history of the Universe. Therefore, matching all the quantities to the data can strongly constrain the evolutionary models for the early Universe.

3. Constructing stellar population models

Synthetic stellar populations models were first used by Tinsley in the 70's and then later developed by Bruzual (1983). Since then many theoretical libraries have become available (e.g. Yoshii & Takahara 1988; Bruzual & Charlot 1993; Worthey 1994)

In order to compute the spectral evolution of galactic stellar populations we used a new set of synthetic stellar population models that are an updated version of the previous models constructed by Jimenez et al.

(1998). The new models are based on the extensive set of stellar isochrones computed by Jimenez et al. (1998) and the set of stellar photospheric models computed by Kurucz (1992) and Jimenez et al. (1998). The interior models were computed using JMSTAR15 (Jimenez et al. 1998) which uses the latest OPAL95 radiative opacities for temperatures larger than 6000 K, and Alexander’s opacities (private communication) for T below 6000 K. For stellar photospheres with temperatures below 8000 K we have used a set of models computed with an updated version of the MARCS code (U. Jørgensen, private communication). We included in these models all the relevant molecules that contribute to the opacity in the photosphere. Stellar tracks were computed self-consistently, i.e. the corresponding photospheric models were used as boundary conditions for the interior models. This procedure has the advantage that the stellar spectra are known at any point along the isochrone and thus the interior of the star is computed more accurately than if a grey photosphere were used. Therefore we overcome the problem of using first a set of interior models computed with boundary conditions defined by a grey atmosphere and then a separate set of stellar atmospheres, either observed or theoretical, that is assigned to the interior isochrone *a posteriori*. The problem is most severe if observed spectra are used because metallicity, effective temperature and gravity are not accurately known and therefore the position assigned for the observed spectra in the interior isochrone may be completely wrong (in some cases the error is larger than 1000 K). A more comprehensive discussion and a detailed description of the code can be found in Jimenez et al. (1998).

An important ingredient in our synthetic stellar population models is the novel treatment of all post-main evolutionary stages that incorporates a realistic distribution of mass loss (see Jimenez et al. (1998) for a full discussion). Thus the horizontal branch is an extended branch and not a red clump like in most other stellar population models. Also the evolution along the asymptotic giant branch is done in a way such that the formation of carbon star is properly predicted as is the termination of the thermal pulsating phase.

Using the above stellar input we compute synthetic stellar population models that are consistent with chemical evolution. The procedure to build stellar populations consistent with chemical evolution was as follows:

We start by constructing simple synthetic stellar populations (SSP). We define an SSP to be a population with homogeneous metallicity and with no further star formation activity, i.e. all the available gas was exhausted in the first star formation episode. The initial star formation episode has a duration no longer than 1% of the age of the SSP. The procedure to build an SSP is the following:

1. A set of 10^6 to 10^{12} (depending on the mass of the population in the model) stellar tracks from our library is distributed according to an initial mass function (IMF).
2. Next, we find the points in the plane of T_{eff} vs. Luminosity where the previous tracks have the required age for the SSP that we want to model. We then produce a synthetic color-magnitude diagram of the SSP.
3. To each point of this synthetic color-magnitude diagram we assign the corresponding self-consistent photospheric model. We finally add all the individual spectra to produce the integrated spectrum of the SSP.

The main advantage of this approach is that it is free of under-sampling problems in the fastest stages of stellar evolution and that it allows the construction of realistic synthetic color-magnitude diagrams since the procedure simply mimics the nature. SSPs are the building blocks of any arbitrarily complicated population since the latter can be computed as a sum of SSPs with variable IMFs and metallicities. Thus, the total galactic luminosity can be computed as:

$$L_{\lambda}(t) = \int_0^t \int_0^{M_f} \int_{Z_i}^{Z_f} SFR(Z, M, t_1) l_{\lambda}(Z, M, t - t_1) dZ dM dt_1 \quad (6)$$

where $l_{\lambda}(Z, M, t')$ is the luminosity of a star of mass M , metallicity Z and age t' , t is the age of the population to be modeled, Z_i and Z_f are the initial and final metallicities respectively of the population, M_f is the largest stellar mass in the population and SFR is the star formation rate that depends on the mass, metallicity and age of the population. In order to compute the SFR it is necessary to know the mass function as a function of time, the evolution of the metallicity in time (*which we properly take into account using our chemical evolution models*) and the amount of gas left in the galaxy to form stars that is also properly accounted for by using the chemical evolution models. For most of the cases it is possible to split the SFR into two factors:

$$SFR(Z, M, t) = \Phi(M, t) \times g(Z, t) \quad (7)$$

where Φ is the mass function and g is the fraction of gas available at any time at the appropriate metallicity consistent with chemical evolution to form stars. Since an SSP is:

$$SSP_{\lambda}(Z, t - t_1) = \int_0^{M_f} \Phi(M, t) \times l_{\lambda}(Z, M, t - t_1) dM \quad (8)$$

then we obtain:

$$L_{\lambda}(t) = \int_0^t \int_{Z_i}^{Z_f} g(t_1, Z) SSP_{\lambda}(Z, t - t_1) dZ dt_1 \quad (9)$$

The approach is fairly straightforward and allows the construction of a large atlas of synthetic stellar population models. Using this approach we have computed an atlas of synthetic stellar population models for ages between 1×10^6 to 1.5×10^{10} years with a range in metallicities from $Z = 0.0001$ to $Z = 0.1$, i.e. from $0.01Z_\odot$ to $5Z_\odot$. Our models have been extensively used to study related problems (e.g. Dunlop et al. 1996, Spinrad et al. 1997), and a detailed comparison with other SSP models in the literature can be found there.

4. Modeling galaxy evolution

4.1. Individual galaxy evolution

In order to compute the evolution of an individual galaxy, we constructed an atlas of synthetic population models in the following way:

1. 5 different morphological types are used: E/S0, Sab, Sbc, Scd, Sdm/Irr. For Sab, Sbc and Scd we separate the contribution from the bulge and the disc. The bulge is always modeled as a high metallicity object with a fixed metallicity of $1.5 Z_\odot$ that was formed at the redshift of galaxy formation (see below) in a star burst of duration 0.1 Gyr. Early type galaxies are modeled so that they reproduced the fundamental plane relations. As is well known star burst models produce evolution for spheroids and ellipticals which is too red because the UV excess (upturn shortwards of 2000Å) observed in these systems (Bertola, Capaccioli & Oke 1982) is not present (Dunlop 1989). In order to compensate for this deficit/excess we introduced a population of very blue (horizontal branch like) stars that reproduces the present day UV excess in spheroids and ellipticals (see Fig. 1). We note that the origin of the UV excess is still a question of open debate, and hence without entering in the origin of the UV excess, we simply adopt the previous empirical approach in order to reproduce the observed UV excess of today's spheroids and ellipticals.
2. Each morphological type is modeled in accordance with chemical evolution. The evolution of the global metallicity is followed by taking into account detailed nucleosynthesis prescriptions by including the contributions to galactic chemical enrichment by stars of all masses (see Matteucci & Francois 1989). The ellipticals are all formed in a very short star burst with a duration of 0.1 Gyr, this short time-scale is required in order to reproduce the observed tight color-magnitude and Mg-Fe relation (Matteucci & Greggio 1986) observed in present-day ellipticals and the wind model is used for their

chemical evolution (Matteucci & Greggio 1986; Arimoto & Yoshii 1987; Arimoto, Yoshii & Takahara 1992) i.e. star formation stops when the remaining gas is blown away by the high supernovae activity. This model is successful in reproducing today’s abundances of ellipticals. The population of ellipticals is formed with a metallicity spread that reproduces the fundamental plane properties (see next section). Discs are assumed to form as primordial gas that accretes around the bulge. We compute the initial surface density of the discs assuming they are well described by isothermal spheres (Fall & Efstathiou 1980; Kashlinsky 1982) with spin parameters for the dark halo $\lambda_{\text{spin}} = 0.03, 0.05$ and 0.07 for Sab, Sbc and Scd respectively. We take the typical half-radius of the model to be representative of the galaxy since we are modeling galaxies as point sources and are not interested in the radial dependence. We assume that the infall rate is higher in the center than in the outermost regions of the disc and is proportional to $\exp(-t/\tau)$, where t is the age of the population and τ is the typical time for the formation of the disc (we adopted $\tau = 2, 4, 7$ and ∞ for Sab, Sbc, Scd and Sdm/Irr respectively). The star formation rate is assumed to depend on both the surface gas density, $\Sigma_g(t)$, and the total surface mass density of the luminous material, $\Sigma_m(t)$. In particular, we adopted a law of the type $g(t) = \nu[\Sigma_g(t)]^{k_1}[\Sigma_m(t)]^{k_2}$ with $k_1 = 1.5, k_2 = 0.5$ and $\nu = 1 \text{ Gyr}^{-1}$ (where this value for ν is the best found for the Galaxy (Chiappini, Matteucci & Gratton 1997)) which is essentially the Schmidt law for star formation in the present-day disks. We further assume that the star formation law is universal.

3. We adopted a Salpeter IMF ($x_s = 1.35$) for bulges and E/S0 and a Scalo IMF (Scalo 1986) for the discs of Sab, Sbc and Scd as well as for Sdm/Irr. For disk galaxies the proportions of the stars with each IMF were taken to be like those of bulge to disk masses.
4. No absorption by dust has been included in the modeling.

Fig.1 shows the spectrum for the different galaxy types according to the adopted prescription. E/S0 galaxy spectrum is shown for $1.5Z_\odot$ which as discussed in the next section corresponds to the metallicity of an L_* galaxy. The dotted lines show the spectrum 1 Gyr after the first burst of star formation and solid lines show the spectrum 14 Gyr after the first star burst. Fig. 1 shows that the strongest effect in the evolution of the spectra for the different morphological types occurs in the region below 4000 Å. The reason for this is that the position of the main sequence turn off of the population is the most sensitive point to changes in age and metallicity (i.e. different star formation schemes) while the giant branch position remains basically the same. 90% of the light in the region below 4000 Å comes from stars near the main

sequence turn-off and below, while beyond 5000 Å the population is dominated by stars from the giant branch and the dwarfs. For Sdm/Irr there is very little evolution with time since they have continuous star formation and therefore there is a continuous reservoir of gas to form young and bright stars. On the contrary, for E/S0 the time evolution is the strongest among all morphological types since their gas reservoir is exhausted after the first star burst. Therefore the population in early type galaxies evolves like $\text{Luminosity} \propto \text{age}^{-3}$ on the main sequence, i.e. in the region below 4000 Å. Indeed at later epochs (age > 10 Gyr) the horizontal branch will make a significant contribution since it will become extended into the blue bands.

4.2. Normalizing early-type galaxies to the fundamental plane

The previous section described the luminosity evolution of individual galaxies for the various galaxy types. The luminosity history depends on both the galaxy age and its metallicity; the dependence is stronger in the visible bands. In principle, for late type galaxies for which we model chemical evolution, the galaxy luminosity at the relevant epochs is practically independent of the initial metallicity. But for early type galaxies (E/S0), which are assumed to have undergone only the initial burst of star formation and to have remained at the value of Z produced in the brief initial burst of star formation (e.g. until the wind from supernovae exhausted the available gas for forming stars) the dependence on the metallicity is more important. Indeed, as the (initial) metallicity changes between $0.01Z_{\odot}$ and $2Z_{\odot}$, the B -band luminosity changes by almost 2 magnitudes by about 12 Gyr after the burst. In the K -band the dependence is weaker, but must nevertheless be corrected for.

Therefore, we have to normalize the early type galaxies to a particular value (or set of values) of Z . The simplest assumption would be to choose a particular and constant value of Z for all early type galaxies. However, this would not be in agreement with observations indicating substantial variations in metallicity among the early type galaxies. Furthermore, with this assumption it would be difficult to reproduce the fundamental plane relations between the central velocity dispersion (σ) and the blue photometric radius of early type galaxies (Dressler et al. 1987; Djorgovski & Davis 1987).

The B -band fundamental plane relations imply that the blue band mass-to-light ratios of early type galaxies scale with the blue luminosity as $M/L_B \propto L_B^{\kappa}$ with $\kappa \simeq 0.25$ (Jorgensen, Franx & Kjaergaard 1996). The mass here refers to the total mass inside the photometric radius where it is dominated by stellar populations. One could be tempted to account for this on the basis of different ages for stellar populations

in the different luminosity (or mass) early type galaxies. However, since at late times ($t \gg \tau$) the blue luminosity $L_B \propto t^{-1}$, reproducing the fundamental plane relations would require gaps of ~ 10 Gyr between formation of (or the first star burst in) the low-luminosity ellipticals and the bright ones.

A plausible alternative assumption, which will also allow us to normalize the metallicity for the early type galaxies, is to assume that the fundamental plane relations reflect the difference in metallicities, rather than age, along the luminosity sequence of ellipticals. The differences in metallicity would imply systematic variations in the IMF as function of galaxy's mass. Since, the bulk of metals produced in the initial burst come from massive stars, the necessary variations arise only from the massive end of the stellar mass function. This hypothesis is not new and was widely discussed elsewhere (Renzini & Ciotti 1993; Worthey, Trager & Faber 1996; Franx et al. 1997). In order to reproduce the fundamental plane relations within the framework of our models and thereby normalize the early-type galaxies to observational data on the fundamental plane we need to be able to reproduce (within the framework of our models) also the recent data on the fundamental plane in K (Pahre, Djorgovski & De Carvalho 1995) which indicate that $M/L_K \propto L_K^{0.16}$. Therefore, the metallicity variations along the mass sequence of the early type galaxies should reproduce $L_B \propto L_K^b$ with $b = 1.16/1.24 \simeq 0.9$. In addition, the recent measurements of the fundamental plane evolution out to $z \sim 0.5$ (or $\simeq 1/3$ look-back-time) indicate that the logarithmic slope of the dependence remains the same while the amplitude (or mass-to-light ratio) changes (Kelson et al. 1997).

The left panel of Fig.2 shows the dependence of the blue-luminosity on the metallicity for the models considered in this paper. The lines are drawn for three values of the time elapsed since the star burst: 9, 12 and 14 Gyr. The middle panel shows the dependence of the K -band luminosity on Z and the right panel shows the corresponding L_B vs L_K relation for the same metallicity galaxies. The net result is that it is possible to account for the fundamental plane relations within the framework of our models if one considers early-type galaxies to span the range from about $0.15Z_\odot$ to $2.5 Z_\odot$ for systems older than 9 Gyr. If the time elapsed since the last star burst is as short as 9 Gyr this would shift the span of metallicities from $\simeq 0.1Z_\odot$ to $1.5Z_\odot$. In any case, the covered span is consistent with the range of metallicities observed in elliptical galaxies. Furthermore, the increase in the L_B (or L_K) due to aging of stellar populations that we find between 5 and 14 Gyr is consistent with the measurements of the fundamental plane relations out to $z \sim 0.6$ (Kelson et al. 1997; Jorgensen et al. 1997).

We therefore normalize our early type galaxies so that they reproduce the fundamental plane relations by varying their metal content along the mass sequence. For normalization point we choose an L_* galaxy to

have absolute blue luminosity $M_{B,*} = -19.8 + 0.5 \lg h$ (Loveday et al. 1992) and central velocity dispersion $\sigma_* = 225$ km/s (Davies et al. 1983). The metallicity of the L_* galaxy is adopted from the Mg- σ relation for ellipticals (Bender, Ziegler & Bruzual 1996) to be $1.5 Z_\odot$.

4.3. Normalizing to the epoch of galaxy formation

The previous two sections specify evolution of the individual galaxies of both early and late types once the IMF of stellar populations is assumed. In our computations we adopt the IMF for the various galaxy types as discussed in Section 4.1, but note that the results depend somewhat strongly on the assumed IMF. Our adopted IMF is motivated by reproducing the chemical abundances of the Galaxy and ellipticals. According to this we chose the Scalo IMF for the disc systems that is the one that best reproduces the chemical gradients in the Galaxy (Chiappini, Matteucci & Gratton 1997); likewise the Salpeter IMF is more appropriate to reproduce the abundances of ellipticals (Bender, Ziegler & Bruzual 1996).

Fig.3 shows the time evolution of the B, I, K luminosities with time since the first burst of star formation. The three bands were chosen since in the rest frame of the galaxy they reflect emission by very different stellar populations. K band is dominated by emission from old stellar populations, B band is dominated by emission from the young hot stars and the I band emission reflects stars of the intermediate mass and age. In particular the B band reflects the current star formation activity in the population since 80% of its light is dominated by the brightest stars on the main sequence turn-off; therefore the younger the stars the smaller M_B . On the other hand K band is purely dominated by stars in the hydrogen shell and double shell burning stages, i.e. the red giant and asymptotic branch as well as by the dwarfs. Since the evolution along these stellar stages is weakly dependent on time, it is expected that M_K evolves very little, in agreement with Fig. 3.

One can see that at late times ($t > \tau$) the blue band luminosity decreases linearly with time. This was discussed by Tinsley (1980) who found that for Salpeter IMF with logarithmic slope x_s the blue luminosity at late times is $L_B \propto t^{1.3-0.3x_s}$. This dependence is a consequence of the fact that for Salpeter IMF the total blue luminosity at any given time is dominated by the luminosity from the most massive stars still on the main sequence, while the lifetime of the stars in this mass range is $t \propto l_{star}^{-1.25}$. On the other hand Sdm+Irr are dominated during their whole lifetime by very massive and new born stars ($M > 10M_\odot$). In K band the luminosity changes at late epochs very little with time as is to be expected in the bands that are dominated by stellar populations whose change in luminosity during the Hubble time is small, i.e. giant

branches and dwarfs on the main sequence. Since, the K band at the same time probes the bolometric luminosity, this means that the total luminosity emitted by galaxies in their rest frame changes little at late times.

The right panel on the top of Fig.3 shows the evolution of the total blue mass-to-light ratio of galaxies plotted in solar units for various galaxy types. Solid line plots the evolution of the L_* early type galaxy, which has roughly the solar metallicity. One can see that the mass-to-light ratio is the highest for early type galaxies and decreases with increasing τ . This trend is in agreement with observations of the stellar mass-to-light ratios in galaxies (e.g. Faber & Gallagher 1979). One can use the plot to constrain both the age of the Universe and the epoch of galaxy formation (cf. Franx et al. 1997). Indeed, the models indicate that at late times $M/L_B \simeq At(\text{Gyr})$ where $A = 1.6, 1.4, 0.85, 0.57, 0.3$ solar units for E/S0, Sab, Sbc, Scd, Sdm+Irr types respectively and time is measured in Gyr. Observations indicate that the blue mass-to-light ratios for stellar components of galaxies today are $\simeq 16h, 12h, 9h, 7h, 2h$ for the same type galaxies (Faber & Gallagher 1979). This implies that the age of the galaxies must be $t(\text{Gyr}) \simeq (10-12) h\text{Gyr}$ old requiring a high (and same for all type galaxies) redshift of galaxy formation. (It is interesting to note that the age of galaxies derived from this argument scales as h whereas the age of the Universe scales as h^{-1}). The K band mass-to-light ratio varies very little with time after $\sim 5\text{Gyr}$ since the initial burst of star formation. There is also little variation with the morphological type. E.g. at $\sim 10\text{Gyr}$ the difference between E/S0 and Scd+Irr galaxies is only ~ 0.5 mag or about a factor of 1.6 in the M/L_K . This is consistent with observations (cf. Table 2 of Faber & Gallagher 1979). Furthermore, our models give $M/L_K \simeq 2$ for L_* elliptical galaxies after 10 Gyr consistent with observational value of $\sim 3h$ (Van Dokkum & Franx 1996).

Fig.4 plots the evolution of the luminosity density at three wavelengths: 0.28, 0.44 and 1 micron for the galaxy evolution specified in this section. In producing the lines in Fig.4 we further assumed that the number density of galaxies is given by the present day blue luminosity function taken from Loveday et al. (1992). No cosmology was assumed here, i.e. the figure plots the emissivity in the rest-frame of the galaxies. Note that the evolution in time of the luminosity density is in good agreement with previous work by Fall, Charlot & Pei (1996); Totani, Yoshii & Sato (1997).

Fig.5 shows the cumulative star formation rate for the modeling assumed here vs z for the open Universe with $\Omega = 0.2$ and assuming that all galaxies started forming their stellar populations at $z_f = 5$. The cumulative rate was computed by turning $g(t, Z)$ (see section 4.1) into $g(z)$ and using the luminosity function from Loveday et al. (1992). Dashed line corresponds to the star formation from only early type

galaxies and solid line from all galaxies. The data points with the errors bars are measurements of star formation rate from Madau (1997) using local surveys and data from the Hubble deep field for $z > 2$. The two points at $z > 2$ have been corrected to account for dust obscuration (see Madau 1997). Conclusions regarding star formation at high z should be treated carefully since these points may really be only the lower limits for the real star formation rate (see e.g. Dunlop 1997). The agreement is excellent if one assumes that the dashed line reflects the galaxy populations for which the Madau (1997) analysis applies (i.e. predominantly late type galaxies with ongoing star formation). On the other hand, if the $z > 2$ points are only the lower limits, then the solid line would agree as well. Otherwise, the solid line can be easily adjusted to agree with the Madau (1997) data by simply shifting the redshift of formation of E/S0 and bulges to $z > 5$. This would result in a second peak at $z > 5$, which still remains unseen but would be supported by the recent discovery of $z > 5$ galaxies (Spinrad et al. 1998, in preparation) and the lack of other than passive evolution of the fundamental plane (Jorgensen et al. 1997) of E/S0 galaxies. It is obvious then that the infall models can account quite accurately for the high redshift points in the Madau (1997) diagram and, because claims to the contrary have been appearing recently, we feel that it is worth emphasizing that the evolution of the star formation rate with epoch is not a proof for any particular type of hierarchical model and neither is it necessarily related to the spectrum of the initial density field. Rather, it can and, perhaps, should be taken as an indication of the rate at which the gas inside already formed galactic halos is converted into stars.

Zepf (1997) has recently reported the lack of red colors in the field population at moderate redshifts ($z \approx 1$) which he interprets as problematic for E/S0 galaxies forming at $z > 3$. The argument is based on the fact that the purely star-burst model would produce colors for E/S0 that are too red compared to what is observed. Indeed, as previously discussed in section 4.1 the purely starburst model is not a good description of E/S0 since it lacks the UV excess observed in these galaxies. As Dunlop (1989) clearly demonstrated, if one takes the observed spectrum of a $z = 0$ elliptical and simply K-corrects it back to $z = 5$, it will produce colors that are bluer than the purely star-burst model. Therefore, one expects that E/S0 formed at $z > 5$ will follow a track in the color– z plane that is bluer than what the star-burst model predicts. This would bring formation redshift of $z > 5$ for E/S0 in agreement with observations. In addition, Zepf (1997) has also shown that a E/S0 formed at $z > 5$ can be brought in agreement with observations if as little as 5% of the total mass of the E/S0 contributed to late star formation episodes ($z < 1$).

The above calculations carry no cosmological input, only continuing star formation in late type galaxies and (passive) evolution of early type ones with time. In order to put these computations in the cosmological

context one has to specify for how long stellar populations in galaxies have been evolving, or what the epoch of galaxy formation was. For simplicity we will assume that all galaxies formed first stellar populations at the same epoch characterized by the redshift z_f . There is currently enough information to limit the range of possible values of z_f . On theoretical side, the small-scale power in the matter distribution in the currently popular cold-dark-matter (CDM) models requires low redshift of galaxy formation: $z_f \simeq (3\text{-}4)$ if $\Omega = 1$ (Efstathiou & Rees 1988) and even lower in the low- Ω CDM models (Kashlinsky 1993). On the other hand, observations indicate that the redshift of galaxy formation is much higher than that, implying the amount of small scale power in excess of that given by the CDM models (Kashlinsky & Jimenez 1997; Kashlinsky 1998). The highest currently known redshift of quasars, which are believed to be associated with galaxies, is 4.92 (Schneider, Schmidt & Gunn 1991). By now, there exist directly observed galaxies at redshifts higher than that: e.g. the recent record of $z = 4.92$ (Franx et al. 1997) that comes from a gravitationally lensed galaxy was superseded by the recent detection of a galaxy at $z = 5.34$ (Spinrad et al 1998, in preparation) with strong L_α emission. Likewise, existence of galaxies at intermediate redshifts $z \simeq 1.5$ such as 53W091 (Dunlop et al. 1996) and 53W069 (Dunlop 1998) with very old stellar populations of $\simeq 3.5$ Gyr rule out Einstein De Sitter Universe and for open models indicate high redshift of galaxy formation which is uncomfortable for low- Ω CDM models (Kashlinsky & Jimenez 1997). An independent argument in Kashlinsky (1998) based on the fundamental plane properties of early type galaxies and the data on their halo dynamics from the recent X-ray observations requires similarly high value of z_f . In principle, one can model formation of galaxies of different masses at different epochs as required in e.g. CDM-type models. However, this would introduce little difference to most of our results and since we are interested in studying the SSP part of galaxy evolution, in order to accentuate the latter we concentrate primarily on the stellar modeling effects.

The age of the Universe provides another constraint on the values of cosmological constants, $(H_0, \Omega, \Omega_\Lambda)$, and the value of z_f . Using the properties of both the luminosity function and morphology of the horizontal branch it is possible to determine independently the age of the globular clusters. Thus, Jimenez et al. (1996) and Jimenez & Padoan (1998) have computed the age for the oldest globular clusters and found a robust value of 12-14 Gyr. This has been recently confirmed by the new Hipparcos data that have determined an accurate distance to some Globular Clusters and thus its age, with current values ranging from 12 to 14 Gyr (Reid 1997) and an absolute lower limit of 10 Gyr. In addition, the Galactic disc contains stars older than 10 Gyr (Jimenez & Flynn 1997). These ages would be difficult to reconcile with the Einstein De Sitter Universe if the values of the Hubble constant are higher than $50 \text{ km s}^{-1} \text{ Mpc}^{-1}$.

5. Results vs observational data

In modeling galaxy evolution at early times, one usually divides the possible evolutionary tracks into two: luminosity evolution and spectral evolution (cf. Yoshii & Takahara 1988). A further evolutionary complication is the possibility of mergers of very early galaxies affecting their stellar populations (Broadhurst, Ellis & Glazebrook 1992). On the other hand, there is a significant bulk of evidence that the dominant evolution comes only from passive stellar evolution in early-type galaxies and the effects of ongoing star formation in late-type ones (e.g. Barger et al. 1998; Driver et al. 1998) since the global counts of galaxies and their redshift distribution can be easily modeled without invoking a population of mergers. We assume here that once the galaxies have formed, the dominant evolution comes from aging stellar populations and the prescribed star formation rate that forms new populations, since as we show these minimal evolution assumptions provide good fits to all the available data.

This in turn means that the comoving number density of galaxies dN in the interval of their present-day luminosity dL remains the same since the epoch of z_f . We normalize the luminosity function of galaxies to the present-day on both the B -band luminosity function from Loveday et al. (1992) and the K -band luminosity function adopted from Gardner et al. (1997).

The morphological mixtures used are the ones from the CfA survey redshift survey with fractions 0.28, 0.19, 0.32, 0.14 and 0.066 for E/S0, Sab, Sbc, Scd and Sdm/Irr respectively (Marzke et al. 1994). These fractions are assumed to remain constant in time.

In the calculations in this section we consider four values of the $z_f = 3, 5, 7, 10$ and adjust the values of the cosmological parameters to reproduce reasonable ages for galaxies and the Universe. We consider cosmologies with $(\Omega, \Omega_\Lambda) = (1, 0), (0.2, 0), (0.2, 0.8), (0.4, 0.6)$; for these parameters, the age of the Universe is $t_0 = (6.6, 8.3, 10.7, 8.7)h^{-1}\text{Gyr}$ respectively. The values of the Hubble constant that we considered are $H_0 = 50, 65, 80 \text{ km/sec/Mpc}$.

5.1. Chemical evolution and $Z(z)$

The first measure of the evolution of stellar populations at early times comes from the measurements of the cosmic metal abundances at high redshifts. Such data are now becoming available.

Pettini et al (1997) have observed a sample of 34 Damped Lyman α systems between redshift $z \approx 0.5$ to 4 and measured their Zn and Cr abundances. Because Zn traces quite closely the iron abundance and

is not depleted by dust as Cr , they then translated Zn abundance into an average metallicity, $\langle Z \rangle$, at the above redshift range. They have also estimated the amount of dust present in these systems and have concluded that systems at high redshifts are much less metal and dust abundant than the Galaxy today (Pettini et al 1997). These measurements provide the most extensive current sample with which we ought to compare our models.

The nature of the DLA systems is still open to debate, since only a few of DLAs have been imaged in order to resolve their morphological nature resulting in normal and Low Surface Brightness galaxies. Nevertheless, it seems appropriate to compare the Pettini et al. (1997) data with the predictions from our model for the discs of Sab, Sbc and Scd since these will be the most likely systems to be responsible for the DLAs. Some caveats should be noted here: firstly, while very important, the Pettini et al. (1997) data still have large error bars and only a weak $z - \langle Z \rangle$ correlation, therefore they may not place very strong constraints on the global evolution of metallicity in the Universe. Secondly, a galaxy is in reality an extended object with different metallicities at different radii. Therefore it is not surprising that Pettini et al (1997) data show a significant dispersion at every redshift, this may be only due to the fact that galactic discs at different radii are responsible of different DLAs.

In this work we are modeling galaxies as source points so at every redshift there is no dispersion. Using the prescriptions for chemical evolution given in section 4.1 and assuming the galaxy mixtures from CfA, it is possible to (re)construct an average galaxy at every redshift and compute the average metallicity. The average metallicity is simply computed by tracking the stellar yields produced by the population at the appropriate time (redshift) and taking into account the inflow of primordial gas falling into the disc (e.g. Matteucci & Francois 1989). Fig. 6 shows the predicted evolution of the averaged metallicity with redshift. It is clear that our model predictions are consistent with the data from Pettini et al. (1997) over the whole redshift range and for all cosmological models. They also reproduce today's average metallicity for the Galaxy.

5.2. Evolution of the luminosity density

We have computed the evolution of the luminosity density as described in section 2 for the cosmological parameters and formation redshifts given at the beginning of this section. The luminosity density was computed in 3 bands $UV = 2200 \text{ \AA}$, $B = 4400 \text{ \AA}$ and $J = 12000 \text{ \AA}$. Fig. 7 shows the evolution of the luminosity density compared with the CFRS data as well as Gallego et al. (1996) and Connolly et al.

(1997). We have normalized our models to the present day luminosity function in B (see section 2). Solid lines correspond to $z_f = 3$, dotted lines to $z_f = 7$ and dashed lines to $z_f = 10$; in all cases we used $H_0 = 65 \text{ km s}^{-1} \text{ Mpc}^{-1}$.

The agreement in most cases is quite good and for zero cosmological constant the lines always pass inside the error bars in all 3 bands. This is indeed a success of the modeling since the UV band is very sensitive to the current star formation while the J band is sensitive to the old stellar and weakly evolving population. On the other hand for $\Omega = 0.2$ and $\Omega_\Lambda = 0.8$ the predicted UV flux lies below the observed data. The reason for this is that in this Universe galaxies are older at all redshifts compared with the open model. In this we differ from the results by Totani, Yoshii & Sato (1997) who find that only flat $\Omega = 0.2$ and $\Omega_\Lambda = 0.8$ model can account for the observed CFRS data thereby ruling out all other cosmological models. On the other hand, there is good agreement with Fall, Charlot & Pei (1996) who find numbers similar to those in Fig. 7 for the Einstein-De Sitter Universe, but using a different approach to compute the emissivity. The difference between Fall, Charlot & Pei (1996) and our models, on the one hand, and Totani, Yoshii & Sato (1997) on the other can be entirely due to different assumptions about the IMF and the chemical evolution. This is known to lead to very different predictions for the evolution of the luminosity density. As an example we show with thick line in the $(\Omega, \Omega_\Lambda) = (0.2, 0)$ panel of Fig. 7 the evolution of the luminosity density for J band using a Scalo IMF for the whole population of galaxies. It is clear that the prediction overshoots the data as previously noted by Madau (1997). But the important point to note here is that with certain freedom in the choice of the IMF (and thus the chemical evolution law) it is possible to bring the $\Omega = 0.2$ and $\Omega = 0.8$ model in agreement with the CFRS data.

We also used the K band normalization to compute the luminosity density and found only about 5% difference, therefore both luminosity functions give a consistent picture and most likely trace the same populations of the modern day galaxies.

5.3. Deep galaxy counts

Recent years have brought wealth of data on galaxy counts down to very faint magnitudes (see Koo & Kron (1992) for a review). In B band the counts go down to $B \simeq 28$ (Metcalfe et al. 1996); in R they go to $R \simeq 27$ (Smail et al. 1995); in I to $I \simeq 26$ (Smail et al. 1995); and the recent measurements in K using the NICMOS array on Keck telescope extended the previous measurements (Cowie, Songaila & Hu 1991) to $K \simeq 24$ (Djorgovski et al. 1995). Further measurements come from the redshift distribution of galaxies at

faint magnitudes in B and K bands (e.g. Songaila et al. 1994, Cowie et al. 1996, Glazebrook et al. 1995). Up to now the general view was that it is very difficult to reconcile B and K counts within the framework of stellar evolution of one galaxy population. This has lead to construction of models with extra population of galaxies at high redshifts (Cole, Treyer & Silk 1992, Babul & Rees 1992) which by now have either died or merged into the observed populations.

The four panels in Fig.8 plot the latest compilation of the data on deep galaxy counts in the four bands, B, R, I, K . The lines show theoretical fits from our models; all the lines are shown for $H_0 = 50 \text{ km s}^{-1} \text{ Mpc}^{-1}$. Larger values of the Hubble constant will leave less time for the evolution of stellar populations, making galaxies brighter (cf. Fig.3). However, we find that the differences in the predicted count values are small and we do not plot lines with higher values of H_0 in the already condensed Fig.8. Solid lines correspond to the Einstein De Sitter Universe, $\Omega = 1, \Omega_\Lambda = 0$; dotted lines to open Universe with $\Omega = 0.2$, and dashed and dashed-dotted lines correspond to flat Universe with cosmological constant $\Omega_\Lambda = 0.8$ and 0.6 respectively. Einstein De Sitter Universe predicts deficient numbers for the counts at faint magnitudes in all bands. This happens for several reasons: the cosmic time allowed for evolution is the smallest here; the volume at high redshifts is small reflecting both the Euclidian space and short cosmic time; and finally in the given magnitude range the galaxies are shifted to lower redshifts in the Einstein De Sitter case leading to further decrease in the volume and time. Open Universe with $\Omega = 0.2$ provides a good fit to K counts, but passes through the lower end of error bars of the data at the faintest magnitudes in other bands. A slightly lower value of Ω in the open Universe will further improve the fit to the data.

The numbers in Fig.8 are shown for $z_f = 5$. For lower values of z_f all the curves will lie under the data at all bands, whereas for higher values of z_f the fits for low Ω models would become even better. As discussed earlier in the paper, such high redshifts of galaxy formation are indeed supported by the recent observations. The theoretical models shown in Fig.8 were normalized to the present galaxy luminosity function in B taken from Loveday et al. (1992). An alternative normalization (particularly in the K counts calculations) is to the data on the present day galaxy luminosity function in K determination of which has recently become possible. We also computed the counts in models normalized to the present-day K band luminosity function taken from Gardner et al. (1997). This gave essentially the same numbers as for the B luminosity function arguing for both the consistency of our results and the fact that the two bands, B and K , likely map the same galaxy populations.

A further test of the models and constraints on the cosmological parameters comes from the redshift

distribution of the counts. Such information is currently sparse, but should become more abundant with the advent of new adjusted optics telescopes. The top two panels in Fig.9 plot the fits of the $\Omega = 0.2$ models to the data in K and B bands. The data are taken for $17 < K < 18$ from Songaila et al. (1994), and for $22.5 < B < 24$ from Glazebrook et al. (1995) (solid lines) and Cowie et al. (1996) (dotted line). As the figure shows, theoretical lines based on our models for $\Omega = 0.2$ Universe provide good fit to the data. The good fits of the models to the available data for both the counts and their redshift distribution are quite encouraging and it is interesting to analyze the redshift distribution of the faintest counts in the blue and K bands. The bottom two panels in Fig.9 show the redshift distribution of the counts from our theoretical models for the Einstein De Sitter Universe (dotted line) and open Universe with $\Omega = 0.2$. The lines are drawn for the faintest magnitude range of the present day K counts (left bottom panel) and B counts. One can see that for the open Universe, which fits the counts, the faintest K counts should be probing galaxies at $z \simeq (4-5)$. For the Einstein De Sitter model which fails to account for the counts, such galaxies would lie at significantly lower redshifts (which in turn could be one of the reasons for the counts deficit in the Einstein De Sitter Universe). The faintest B magnitudes currently available probe galaxy distribution at significantly lower redshifts as the right lower panel of Fig.9 shows.

Indeed a further test on the redshift distribution of faint galaxies comes from their colors, i.e. from photometric determination their redshifts. Djorgovski et al. (1995) have obtained I, g and r colors for the faintest galaxies in their sample (see fig. 4 in Djorgovski et al. (1995)). Our predicted K counts for $23 < K < 24$ extend to redshift 5. At this redshift our models predict $I - K \approx (2-3)$ in excellent agreement with colors measured by Djorgovski et al. (1995); this would imply that galaxies with $23 < K < 24$ are indeed at $z \simeq (4-5)$. On the other hand, if galaxies were not at $z \approx 5$, then their colors (e.g. I-K) should be different than those predicted from galaxy models. Note, however, that ideally one would require more than just two bands for accurate photometric determination of redshifts.

Note that the presence of dust can boost the B band counts, which at the faintest magnitudes probe galaxy populations at $z \simeq (1.5-2.5)$, without significantly affecting the K counts which at the faintest magnitudes probe significantly earlier epochs when little dust had time to form yet (Pettini et al. 1997); this would further improve the open Universe fit to the data. Furthermore, adopting the redshift of galaxy formation $z_f > 5$ would increase the low- Ω curves for the number counts and would also improve fits to the data. We conclude that our models for evolution of galaxies and SSPs give good fit to the data with low $\Omega \simeq 0.2$ and with or without the cosmological constant.

5.4. The near-IR cosmic infrared background from early galaxies

A further measure of galaxy evolution at early times and a subject of intensive searches is the cosmic infrared background produced by them. There exist many calculations of the total levels of the CIB produced by galaxy evolution (e.g. Partridge & Peebles 1967, Stecker, Puget & Fazio 1977, Bond, Carr & Hogan 1986, Franceschini et al. 1991, Fall, Charlot & Pei 1996). The models predict the levels of the CIB in the near-IR around $5\text{-}15 \text{ nWm}^{-2}\text{sr}^{-1}$. Fluctuations in the CIB have been calculated by Wang (1991), Kashlinsky, Mather & Odenwald (1996) and Kashlinsky et al. (1996) and generally give the amplitude of $\sim (5\text{-}10)\%$ on the DIRBE beam scales ($\sim 0.5 \text{ deg}$).

We computed the properties of the CIB in our models from eqs.(4) for the mean level, and from eq.(5) for fluctuations produced by galaxy clustering. Fig.10 shows the rate of the flux production, dF/dz in different bands for our models with $H_0 = 50 \text{ km/sec/Mpc}$. The four panels correspond to the values of z_f written above each box. Solid lines correspond to J band ($1.25 \mu\text{m}$), dotted to K ($2.2 \mu\text{m}$) and dashed lines to L band ($3.5 \mu\text{m}$). Thick lines of each type correspond to $\Omega = 0.2$ and thin lines to the Einstein De Sitter Universe, $\Omega = 1$. The general structure of the figures is the same for all cosmologies, only numerical values (slightly) differ: there is an initial peak corresponding to the initial burst of star formation, where the flux is dominated by the redshifted emission from massive (O,B) stars. After the first massive stars die the flux rate subsides and then for most values of z_f it reaches a dip when the flux is dominated by the galactic spectra redshifted from $\lambda \simeq (3000\text{-}4000) \text{ \AA}$. As Fig.1 shows that there is a sharp drop there for galaxy emission from all types of galaxies (the 4000 \AA break is a blend of several absorption lines); the largest drop is for the early-type galaxies where this part of the spectrum is not replenished by photons from the newly-forming massive stars. For low values of z_f the galaxy rest frame wavelengths of $\lambda < 4000 \text{ \AA}$ do not get shifted into the H, K bands which explains the absence of the dip for the dashed and dotted lines in the $z_f = 3$ panel.

For higher values of the Hubble constant, the galaxies are younger and, hence, brighter at each value of z . This would lead to the rise in the amplitude of the curves in Fig.9, but the overall shape would remain the same. Fig.10 shows the values of the total CIB flux for low (left panel) and high values of the Hubble constant. The fluxes in $\text{nWm}^{-2}\text{sr}^{-1}$ are shown in eight bands: B (0.44 micron), R (0.8 micron), I (0.9 micron), J (1.25 micron), H (1.65 micron), K (2.2 micron), L (3.5 micron) and M (5 micron). At the longest wavelengths there is a significant contribution from dust in the nearby galaxies as well as stellar atmospheres and our flux numbers should be regarded only as lower limits. The different symbols

correspond to the four (Ω, Ω_Λ) different cosmological models considered; thick symbols correspond to $z_f = 3$ and thin symbols to the same value of (Ω, Ω_Λ) and $z_f = 10$. One can see that there is little variation in the total CIB flux with different cosmologies, but at given z_f and H_0 the biggest values of flux come from the low- Ω models which also fit the galaxy counts. Since the less time the galaxies had to evolve the brighter they are at each redshift, the flux values increase with increasing Hubble constant and/or decreasing z_f .

In order to compute the power spectrum of the CIB from eq.(5) we have to input the power spectrum of galaxy clustering today, $P_3(k)$. On small scales ($< 50h^{-1}$ Mpc) it was taken from the APM survey of galaxies in b_J (Maddox et al 1990) with the power spectrum adopted from the Baugh & Efstathiou (1993) de-projection of the APM data on the 2-point angular galaxy correlation data. On larger scales it was assumed to go into the Harrison-Zeldovich regime consistent with the COBE DMR measurements (Smoot et al 1992, Bennett et al 1996). Two regimes of the evolution of galaxy clustering were assumed: clustering stable in proper coordinates, $\Psi^2(z) \propto (1+z)^{-3}$, and $\Psi^2(z) \propto (1+z)^{-2}$ which roughly corresponds to either growth of linear fluctuations in the Einstein de Sitter Universe or clustering pattern with the galaxy two-point correlation function $\xi \propto r^{-2}$ being stable in comoving coordinates. These describe two extremes for the evolution of galaxy clustering (Peebles 1980).

The upper panels in Fig.12 plot the order-of-magnitude fluctuation in four bands (J, H, K, L) on angular scale $\sim \pi/q$ in the CIB flux, $\sqrt{q^2 P_2(q)/2\pi}$ in $\text{nWm}^{-2}\text{sr}^{-1}$, vs q^{-1} shown in arcmins. Thin lines correspond to $H_0 = 50 \text{ km/sec/Mpc}$. Solid lines correspond to the Einstein de Sitter Universe, dotted to the open Universe with $\Omega = 0.2$, dashes to the flat Universe with $(\Omega, \Omega_\Lambda) = (0.2, 0.8)$ and dashed-dotted lines to $(\Omega, \Omega_\Lambda) = (0.4, 0.6)$. Two lines of each type correspond from bottom to top to clustering pattern stable in proper and comoving coordinates. Thick solid line corresponds to $H_0 = 80 \text{ km/sec/Mpc}$. One can see that on scales of about $\pi/q \simeq 0.5 \text{ deg}$ the CIB fluctuations are about 10%. On smaller scales, or large q , they increase with decreasing angular scale as $\propto (q^{-1})^{-0.35}$. On scales above a few degrees the slope of the CIB fluctuations changes since the power spectrum there reflects reflects the initial power spectrum of matter distribution.

Fig.12 shows the contribution to the fluctuations in the CIB from various redshifts. The lower panels show $z(dF/dz)^2 \Delta^2(q(1+z)/x(z))$ which reflects to within a slowly varying factor $\Psi^2(z)/(H_0 dt/dz)$, the rate at which the fluctuations are generated with z . Solid lines correspond to $q^{-1} = 10 \text{ arcmin}$ and dotted lines to $q^{-1} = 1 \text{ degree}$. Thick lines correspond to $z_f = 10$ and thin lines to $z_f = 5$. The numbers are plotted for $H_0 = 50 \text{ km s}^{-1} \text{ Mpc}^{-1}$. One can see that the CIB fluctuations contain information about galaxy

evolution at high and cosmologically interesting redshifts. The range of redshifts contributing to each band fluctuations increases with increasing wavelength and angular scale. The shape of the lines, including the peak at high redshifts and the following dip, is determined by the form of dF/dz .

We therefore find that for models normalized to the data on galaxy counts, one can expect significant CIB fluxes of (10-30) $\text{nWm}^{-2}\text{sr}^{-1}$ in the near-IR bands of J, H, K , which is larger than previous estimates. Likewise, there should be significant and potentially measurable fluctuations in the CIB flux, which on sub-degree scales, are in excess of 10% of the mean flux. The current best limits from the DIRBE all-sky analysis on the CIB (Hauser et al. 1998) and its fluctuations (Kashlinsky, Mather & Odenwald 1996, Kashlinsky et al. 1996) are still above our estimates, but not by a large margin. Note that larger fluctuations could be produced if the dip in dF/dz due to the redshifted galaxy emission originating at $\lambda < 4000 \text{ \AA}$ is filled up. This could be achieved by e.g. a moderate star-burst (5%) at early stages during the beginning of the infall process.

A further constraint on the underlying cosmology and galaxy evolution would come from the measurements of the diffuse extragalactic background in the optical bands. Such measurements were provided recently by Bernstein (1998, preprint) for the mean (DC) level analysis and by Vogeley (1997) from the fluctuations analysis of the Hubble Deep Field. Both give fluxes between 10 and 20 $\text{nWm}^{-2}\text{sr}^{-1}$ in B (0.44 micron) and R (0.81 micron) bands. We computed the predicted flux levels in these bands from our models and these are plotted in Fig. 11 with the same symbols as the near-IR bands. The predicted levels are in good agreement with the Bernstein (1998, preprint) and Vogeley (1997) measurements if the redshift of galaxy formation is high; the numbers for $z_f = 3$ models would produce too much flux in these bands, especially if the Hubble constant is high. It is worth pointing out that because of the Lyman break at 912 \AA in the spectrum of galaxies, the diffuse extragalactic background in the visible bands does not probe as early epochs as those reflected in the CIB.

6. Conclusions

In this paper we considered constraints from and predictions for the early Universe that follow from the evolutionary models of stellar populations in forming galaxies. We constructed accurate synthetic models for the evolution of stellar populations which are assumed to follow the Schmidt law for star formation. In modeling galaxy evolution we further account for chemical evolution. Early type galaxies have been normalized to the fundamental plane relations assumed to reflect variations in the mean metallicity along

the luminosity sequence. Galaxy mixes are adopted from the CfA catalog. We assumed the Salpeter IMF for stars in early type galaxies and bulges of disk galaxies and the Scalo IMF for the disk stellar material. The galaxy numbers were normalized to the present-day galaxy luminosity function measurements in both B and K bands; both give consistent results.

This allowed us to compute parameters that characterize the evolution of stellar populations in the early Universe to be compared with the available observational data. The computations were made for various cosmological density parameters Ω, Ω_Λ and the Hubble constant.

Our main conclusions can be summarized as follows:

- 1) We computed the evolution of the mean cosmic metallicity with z . All models and cosmological parameters provide good fits to the current data. The current data have substantial uncertainties; after these get reduced one can hope to be able to further discriminate between the various models and cosmologies.
- 2) The evolution of the mean luminosity density in the UV, B, J bands is well reproduced in our models, but models with zero cosmological constant are preferred. Our models reproduce well the recent HST data on the evolution of the star formation rate with redshift.
- 3) Our models give good fits to the available data on the deep galaxy counts in all bands where the observations are available, B, R, I, K , for low Ω models (both flat and open Universe). The models thus do not require additional galaxy populations at intermediate and high redshifts in order to explain simultaneously B and K counts. We further fit well the redshift distribution of B and K counts in the magnitude range where such data are available.
- 4) We compute in detail the mean CIB flux produced by this evolution and the power spectrum of the CIB angular distribution. Our predictions are still below the current observational limits, but not by a large factor. This makes us optimistic that both the CIB and its angular structure can be measured in the upcoming years. We also computed the mean flux in the background light from this evolution in the visible bands, B and R , and find that the recent positive measurements of the background at these bands require high redshift of galaxy formation, $z_F \geq 5$.

References

Arimoto N., Yoshii Y., 1987. *A&A*, 173, 23.

Arimoto N., Yoshii Y., Takahara F., 1992. *A&A*, 253, 21.

Babul A., Rees M. J., 1992. *MNRAS*, 255, 346.

Barger et al., 1998. *astro-ph/9801112*, .

Bender R., Ziegler B., Bruzual G., 1996. *ApJ*, 463, L51.

Bertola F., Capaccioli M., Oke J. B., 1982. *ApJ*, 254, 494.

Bond J. R., Carr B. J., Hogan C. J., 1986. *ApJ*, 306, 428.

Broadhurst T. J., Ellis R. S., Glazebrook K., 1992. *Nature*, 355, 55.

Bruzual A. G., Charlot S., 1993. *ApJ*, 405, 538.

Bruzual G., 1983. *ApJ*, 273, 105.

Chiappini C., Matteucci F., Gratton R., 1997. *ApJ*, 477, 765.

Cole S., Treyer M.-A., Silk J., 1992. *ApJ*, 385, 9.

Connolly A. J., Szalay A. S., Dickinson M., Subbarao M. U., Brunner R. J., 1997. *ApJ*, 486, L11.

Cowie L. L., Songaila A., Hu E. M., Cohen J. G., 1996. *AJ*, 112, 839.

Cowie L. L., Songaila A., Hu E. M., 1991. *Nature*, 354, 460.

Davies R. L., Efstathiou G., Fall S. M., Illingworth G., Schechter P. L., 1983. *ApJ*, 266, 41.

Djorgovski S., Davis M., 1987. *ApJ*, 313, 59.

Djorgovski S., Soifer B. T., Pahre M. A., Larkin J. E., Smith J. D., Neugebauer G., Smail I., Matthews K., Hogg D. W., Blandford R. D., Cohen J., Harrison W., Nelson J., 1995. *ApJ*, 438, L13.

Dressler A., Lynden-Bell D., Burstein D., Davies R. L., Faber S. M., Terlevich R., Wegner G., 1987. *ApJ*, 313, 42.

Driver et al., 1998. *astro-ph/9802092*, .

Dunlop J., Peacock J., Spinrad H., Dey A., Jimenez R., Stern D., Windhorst R., 1996. *Nature*, 381, 581.

Dunlop J., 1989. PhD Thesis, University of Edinburgh, .

Dunlop J., 1997. *astro-ph/9704294*, .

Dunlop J., 1998. *astro-ph/9801114*, .

Efstathiou G., Rees M. J., 1988. *MNRAS*, 230, 5P.

Faber S. M., Gallagher J. S., 1979. *ARA&A*, 17, 135.

Fall S. M., Efstathiou G., 1980. *MNRAS*, 193, 189.

Fall S. M., Charlot S., Pei Y. C., 1996. *ApJ*, 464, L43.

Franceschini A., De Zotti G., Toffolatti L., Mazzei P., Danese L., 1991. *Astronomy and Astrophysics Supplement Series*, 89, 285.

Franx et al., 1997. In *The Nature of Elliptical Galaxies*, Editors Arnaboldi, DaCosta and Saha, .

Franx M., Illingworth G. D., Kelson D. D., Van Dokkum P. G., Tran K.-V., 1997. *ApJ*, 486, L75.

Gallego J., Zamorano J., Aragon-Salamanca A., Rego M., 1996. *ApJ*, 459, L43.

Gardner J. P., Sharples R. M., Frenk C. S., Carrasco B. E., 1997. *ApJ*, 480, L99.

Glazebrook K., Peacock J. A., Miller L., Collins C. A., 1995. *MNRAS*, 275, 169.

Hauser et al., 1998. preprint, .

Jimenez R., Flynn C., 1997. *astro-ph/9709056*, .

Jimenez R., Padoan P., 1998. *ApJ*, 480, in press.

Jimenez R., Thejll P., Jorgensen U. G., Macdonald J., Pagel B., 1996. *MNRAS*, 282, 926.

Jimenez R., Dunlop J., Peacock J., MacDonald J., Jorgensen U., 1998. *MNRAS*, submitted.

Jorgensen I., Hjorth J., Franx M., Van Dokkum P., 1997. *Bull. American Astron. Soc.*, 190, #03.02, 190, 0302.

Jorgensen I., Franx M., Kjaergaard P., 1996. *MNRAS*, 280, 167.

Kashlinsky A., Jimenez R., 1997. *ApJ*, 474, L81.

Kashlinsky A., Mather J. C., Odenwald S., Hauser M. G., 1996. *ApJ*, 470, 681.

Kashlinsky A., Mather J. C., Odenwald S., 1996. *ApJ*, 473, L9.

Kashlinsky A., 1982. *MNRAS*, 200, 585.

Kashlinsky A., 1993. *ApJ*, 406, L1.

Kashlinsky A., 1998. *ApJ*, 492, 1.

Kelson et al., 1997. In *The Nature of Elliptical Galaxies*, Editors Arnaboldi, DaCosta and Saha, .

Koo D. C., Kron R. G., 1992. *ARA&A*, 30, 613.

Kurucz R., 1992. CDROM13, .

Lilly S. J., Le Fevre O., Hammer F., Crampton D., 1996. *ApJ*, 460, L1.

Loveday J., Peterson B. A., Efstathiou G., Maddox S. J., 1992. *ApJ*, 390, 338.

Madau P., Ferguson H. C., Dickinson M. E., Giavalisco M., Steidel C. C., Fruchter A., 1996. *MNRAS*, 283, 1388.

Madau P., 1997. *astro-ph/9709147*, .

Marzke R. O., Geller M. J., Huchra J. P., Corwin, Harold G. J., 1994. *AJ*, 108, 437.

Matteucci F., Francois P., 1989. *MNRAS*, 239, 885.

Matteucci F., Greggio L., 1986. *A&A*, 154, 279.

Metcalfe N., Shanks T., Campos A., Fong R., Gardner J. P., 1996. *Nature*, 383, 236.

Pahre M. A., Djorgovski S. G., De Carvalho R. R., 1995. *ApJ*, 453, L17.

Partridge R., Peebles J., 1967. *ApJ*, 148, 377.

Peebles P. J. E., 1980. In: *The large-scale structure of the universe*, Princeton University Press, 1980.

Pettini M., Smith L. J., King D. L., Hunstead R. W., 1997. *ApJ*, 486, 665.

Puget J. L., Abergel A., Bernard J. P., Boulanger F., Burton W. B., Desert F. X., Hartmann D., 1996. *A&A*, 308, L5.

Reid N., 1997. *AJ*, 114, 161.

Renzini A., Ciotti L., 1993. *ApJ*, 416, L49.

Scalo J. M., 1986. *Fundamentals of Cosmic Physics*, 11, 1.

Schlegel D. J., Finkbeiner D. P., Davis M., 1998. *ApJ*, 499.

Schneider D. P., Schmidt M., Gunn J. E., 1991. *AJ*, 102, 837.

Smail I., Hogg D. W., Yan L., Cohen J. G., 1995. *ApJ*, 449, L105.

Songaila A., Cowie L. L., Hu E. M., Gardner J. P., 1994. *ApJS*, 94, 461.

Spinrad H., Dey A., Stern D., Dunlop J., Peacock J., Jimenez R., Windhorst R., 1997. *ApJ*, 484, 581.

Stecker F. W., Puget J. L., Fazio G. G., 1977. *ApJ*, 214, L51.

Tinsley B. M., 1980. *Fundamentals of Cosmic Physics*, 5, 287.

Totani T., Yoshii Y., Sato K., 1997. *ApJ*, 483, L75.

Van Dokkum P. G., Franx M., 1996. *MNRAS*, 281, 985.

Vogeley M., 1997. *astro-ph/9711209*, .

Wang B., 1991. *ApJ*, 374, 465.

Worthey G., Trager S., Faber S. M., 1996. In: *Fresh Views of Elliptical Galaxies*, ASP Conf. Ser. Vol. 86, eds. A. Buzzoni and A. Renzini, 203.

Worthey G., 1994. *ApJS*, 95, 107.

Yoshii Y., Takahara F., 1988. *ApJ*, 326, 1.

Zepf S., 1997. *Nature*, 390, 377.

Figure Captions

Figure 1: Spectra for various galaxy types at 14 Gyr (solid lines) and at 1 Gyr (dotted lines). The evolution with morphological type is stronger in the region below 4000 Å because the main sequence for the new born stars lies in this region. As expected after 1 Gyr since the first burst of star formation all morphological types have very similar spectra.

Figure 2: The left panel shows the change with metallicity (Z) in L_B for an L_* early type galaxy for 3 different ages. The middle panel shows a similar plot but for L_K . The right panel shows the combined evolution of L_B and L_K for the metallicity range plotted in the previous panels. The fact that $L_B \propto L_K^{0.9}$ implies that the properties of the fundamental plane can be reproduced by systematic variations in metallicity with mass for early type galaxies.

Figure 3: The evolution with time for B,I and K magnitudes (shown in arbitrary units) and M/L_B (shown in solar units) for various galaxy types.

Figure 4: Evolution of the comoving luminosity density vs. time at 2800 Å, 4400 Å and 1 μm for all galaxy types weighted with the CfA fractions.

Figure 5: The redshift evolution of the global star formation rate in the universe predicted for our models for late type galaxies (dashed line) and all galaxies (solid line). The data are from Madau 1997. The agreement is excellent if only late type galaxies are considered, but is quite reasonable also for all galaxy types (see text).

Figure 6: The predicted evolution of the averaged metallicity in the Universe for late type galaxies as predicted in our models is compared with Pettini et al. 1997 data for four different cosmologies.

Figure 7: Evolution of the comoving luminosity density vs. redshift at 2800 Å, 4400 Å and 1 μm for all galaxy types weighted with the CfA fractions plotted for 3 different redshifts of galaxy formation. The data are from Lilly et al. 1996, Gallego et al. 1996, Connolly et al. 1997. In all cases the agreement between data and models is excellent, except for the case $\Omega_0 = 0.2$ and $\Omega_\Lambda = 0.8$. In this case the model prediction for the UV is below the observed data since for each z the galaxies are older than in the Einstein De Sitter Universe.

Figure 8: Observed differential counts in several bands and our model predictions. The fits to the counts are excellent for open models in all four bands. The $\Omega_0 = 0.2$, $\Omega_\Lambda = 0.8$ universe overshoots the I counts by a small margin, but otherwise provides good fits. The models have been plotted for $z_f = 5$,

a higher value of z_f would improve the fits for open universes. The prediction for the Einstein De Sitter Universe fail to fit the data by a large margin.

Figure 9: The predicted redshift distribution of counts in B and K is compared with observational data from Songaila et al. 1994 (upper-left panel), Glazebrook et al. 1995 (upper-right panel solid line) and Cowie et al. 1996 (upper-right pane dotted line), the agreement is good in all cases. The two bottom panels show the predicted redshift distribution for the faintest observed B and K counts. Note that galaxies in K counts should extend to redshifts of about 5.

Figure 10: The rate of production of the CIB flux, $z dF/dz$ is plotted vs z for the four redshifts of galaxy formation written above each panel. Solid lines correspond to J band, dotted to K and dashed to L . Thin lines of each type correspond to the Einstein De Sitter Universe and thick lines to $\Omega = 0.2$ and zero cosmological constant. The first peak correspond to the initial burst of star formation with the following dip coming from emission redshifted from 3000-4000 Å .

Figure 11: The total flux for background light produced by the early evolution of galaxies is plotted in eight bands: B, R, I, J, H, K, L, M . Plus signs correspond to the Einstein De Sitter Universe, asterisks to the open Universe with $\Omega = 0.2$, diamond to the flat Universe with $(\Omega, \Omega_\Lambda) = (0.2, 0.8)$ and triangles to $(\Omega, \Omega_\Lambda) = (0.4, 0.6)$. Thick signs correspond to $z_f = 10$ and thin lines to $z_f = 3$. The plots are shown for the two values of the Hubble constant written above each panel.

Figure 12: Top four panels: plot the typical order-of-magnitude fluctuation in the CIB flux, $\sqrt{q^2 P_2(q)/2\pi}$ on scale π/q . It is plotted vs q^{-1} in arcmins for the four near-IR bands shown on top of each panel. Thin solid lines correspond to the Einstein De Sitter Universe; dotted lines to the open Universe with $\Omega = 0.2$; dashed and dashed-dotted lines correspond to the flat Universe with $(\Omega, \Omega_\Lambda) = (0.2, 0.8)$ and $(0.4, 0.6)$ respectively. All thin lines are drawn for $H_0 = 50$ km/sec/Mpc. Two lines of each type correspond to clustering being stable in proper and comoving coordinates from bottom up. Thick solid line corresponds to the Einstein De Sitter Universe with $H_0 = 80$ km/sec/Mpc.

Bottom four panels show $d[q^2 P_2(q)]/dz$ computed from eq.(5) with $\Psi^2(z)d(H_0 t)/dz = 1$. The four panels correspond to the four near-IR bands written above the top panel. Solid lines correspond to $q^{-1} = 10$ arcmin and dotted lines to $q^{-1} = 60$ arcmin. Thick lines of each type correspond to $z_f = 10$ and thin lines to $z_f = 5$.

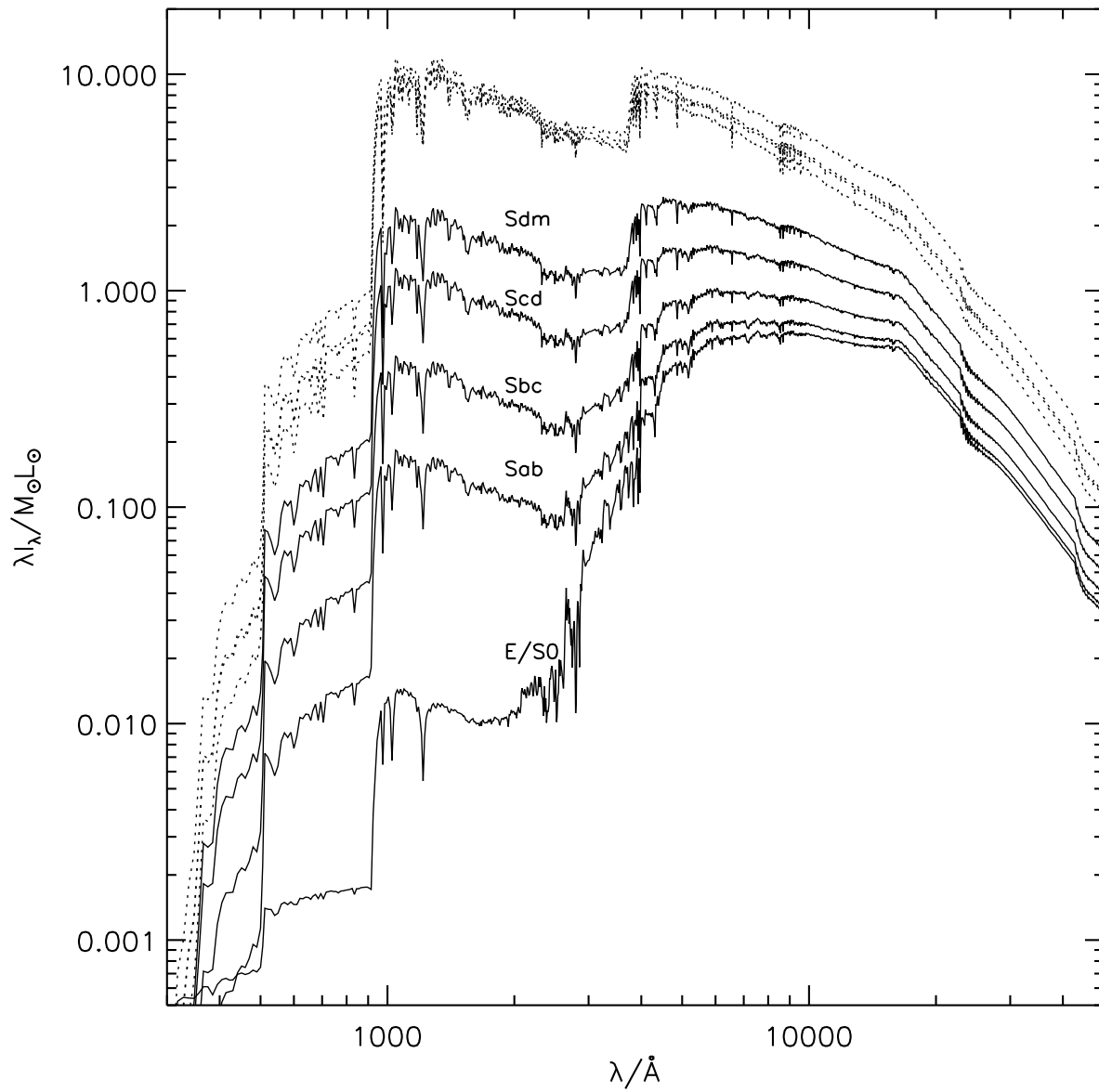


Fig. 1.—

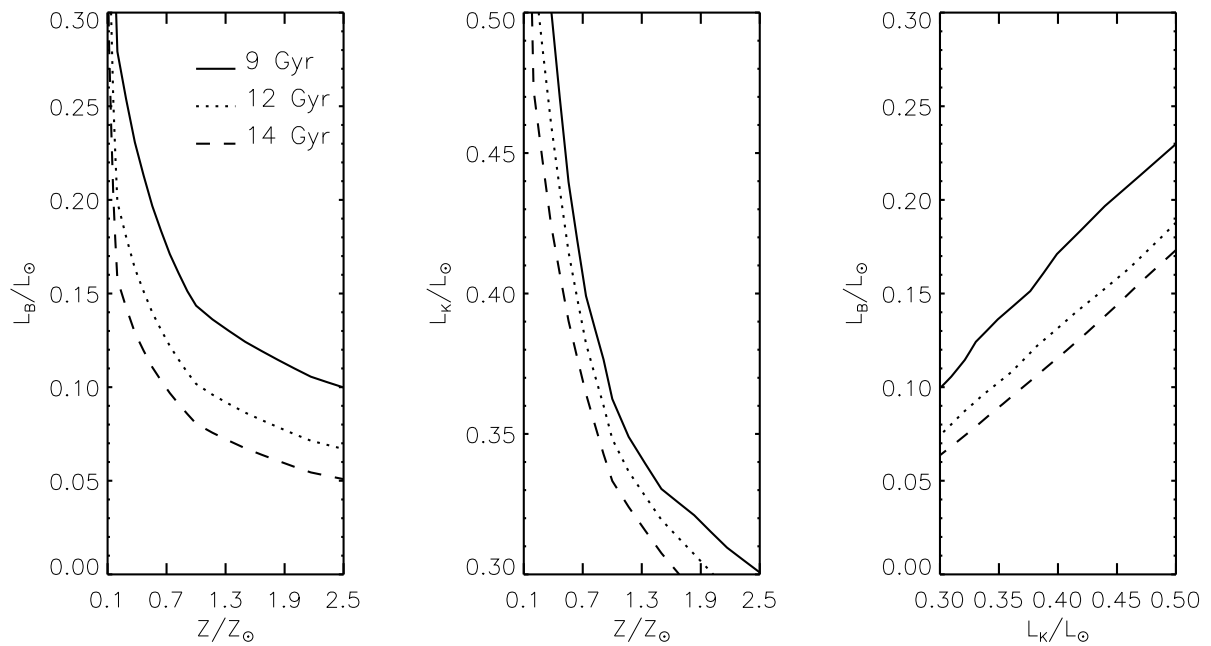


Fig. 2.—

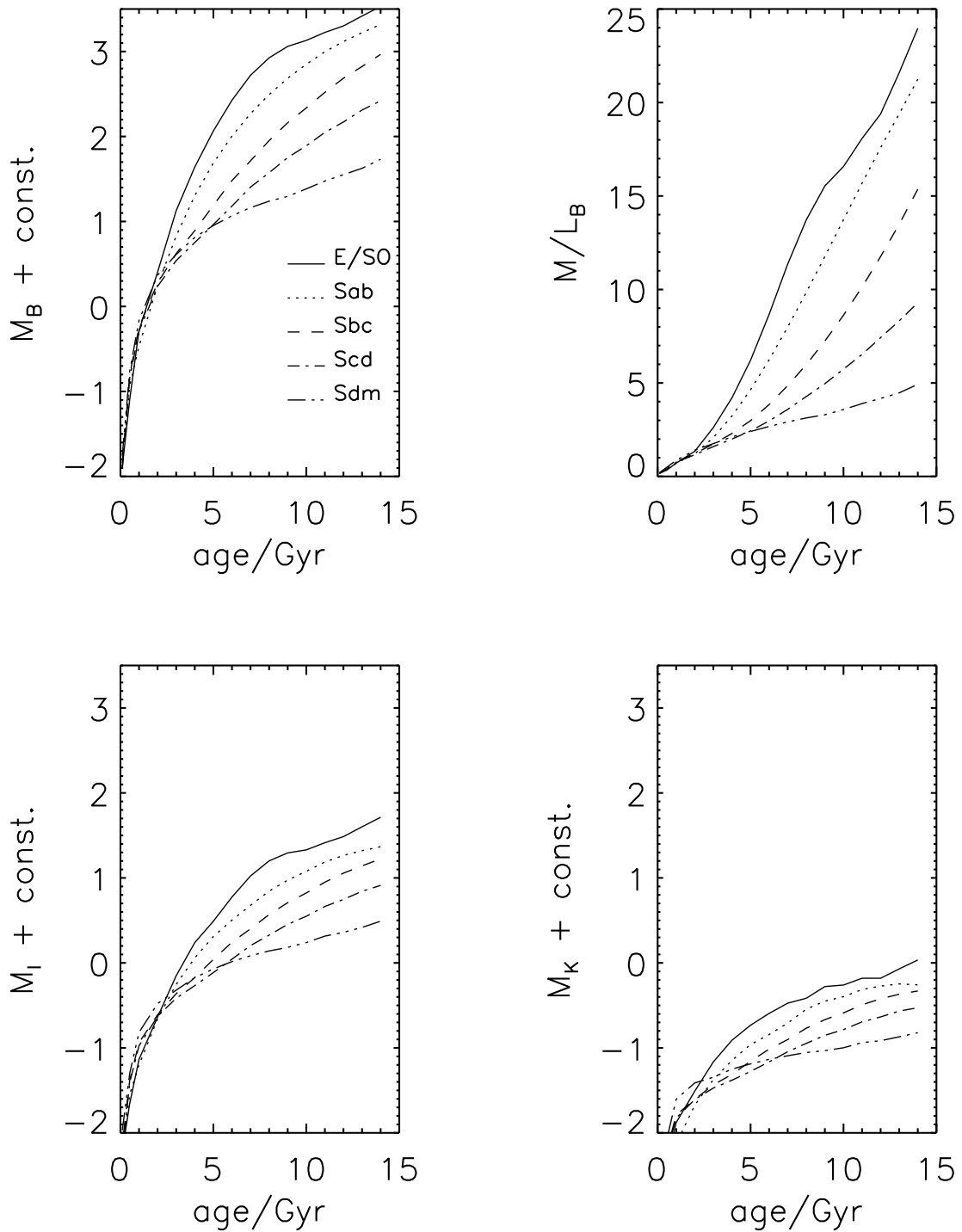


Fig. 3.—

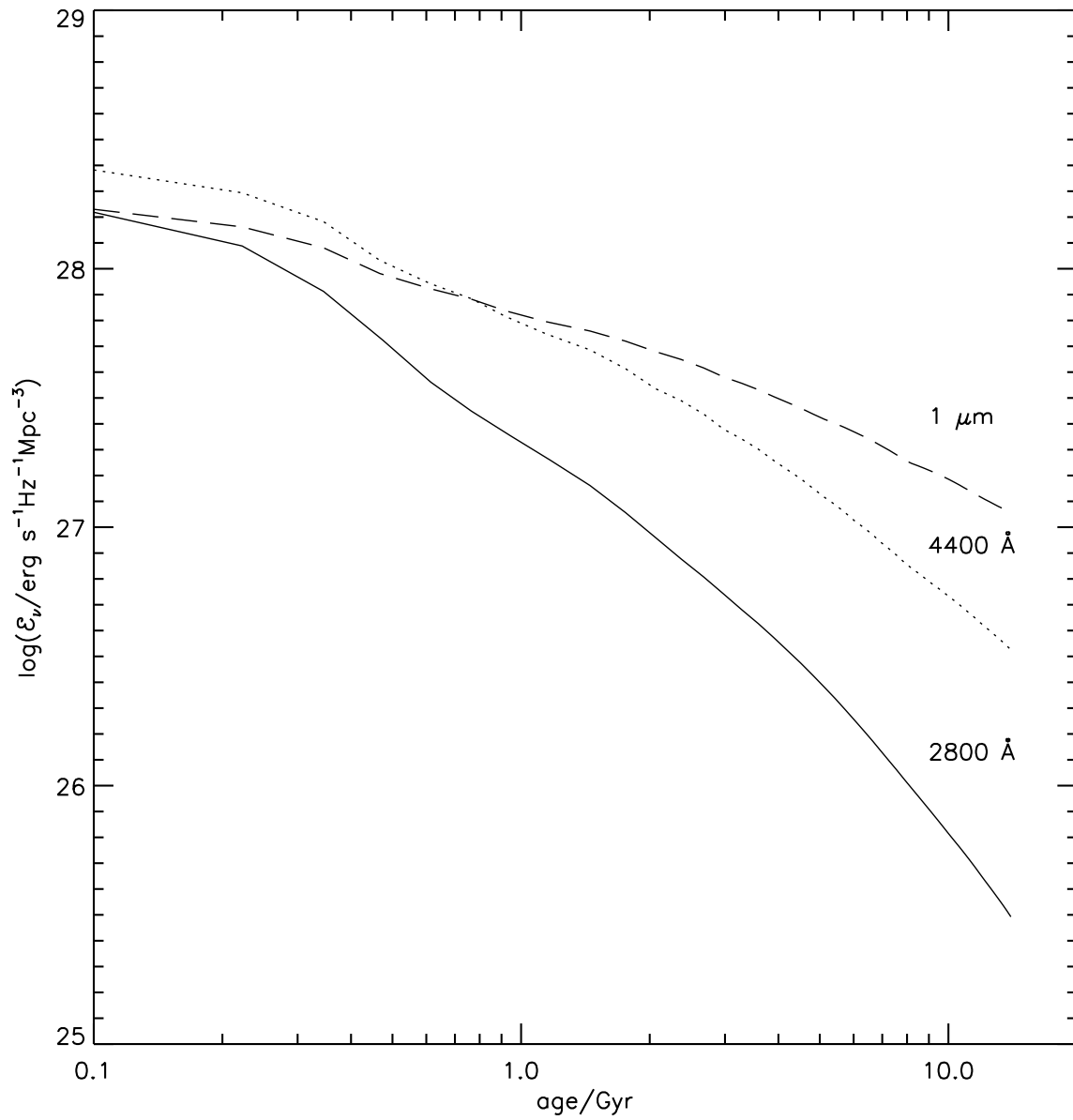


Fig. 4.—

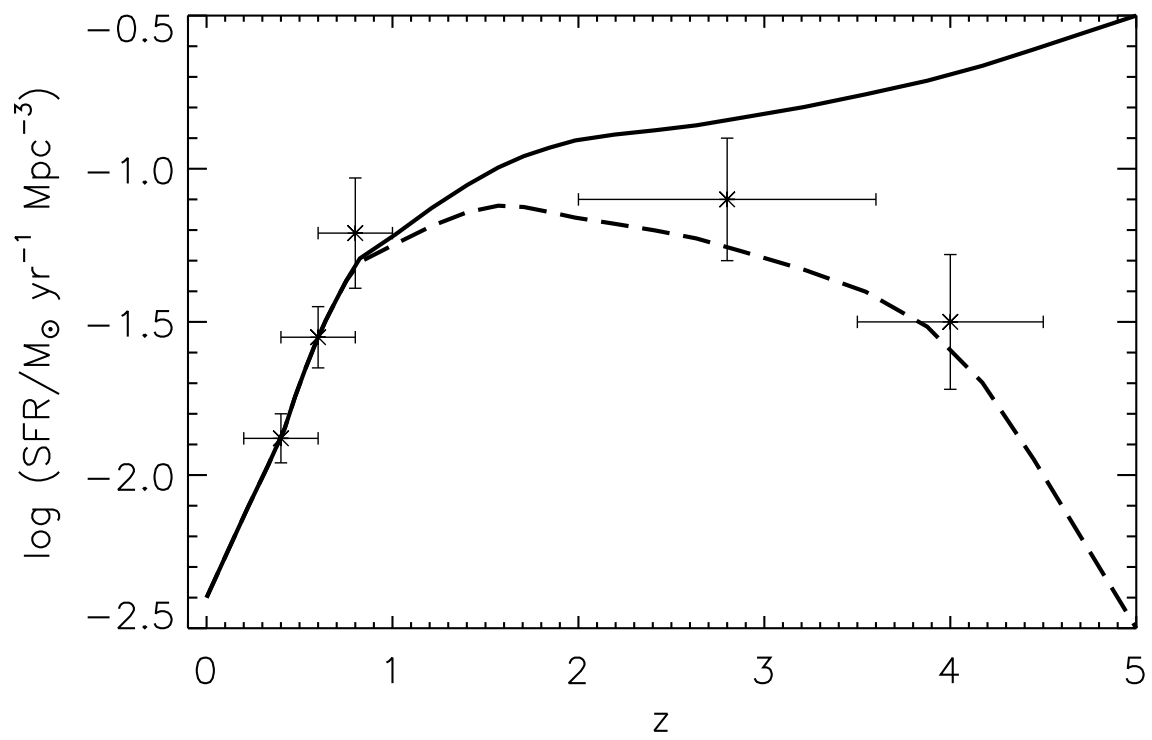


Fig. 5.—

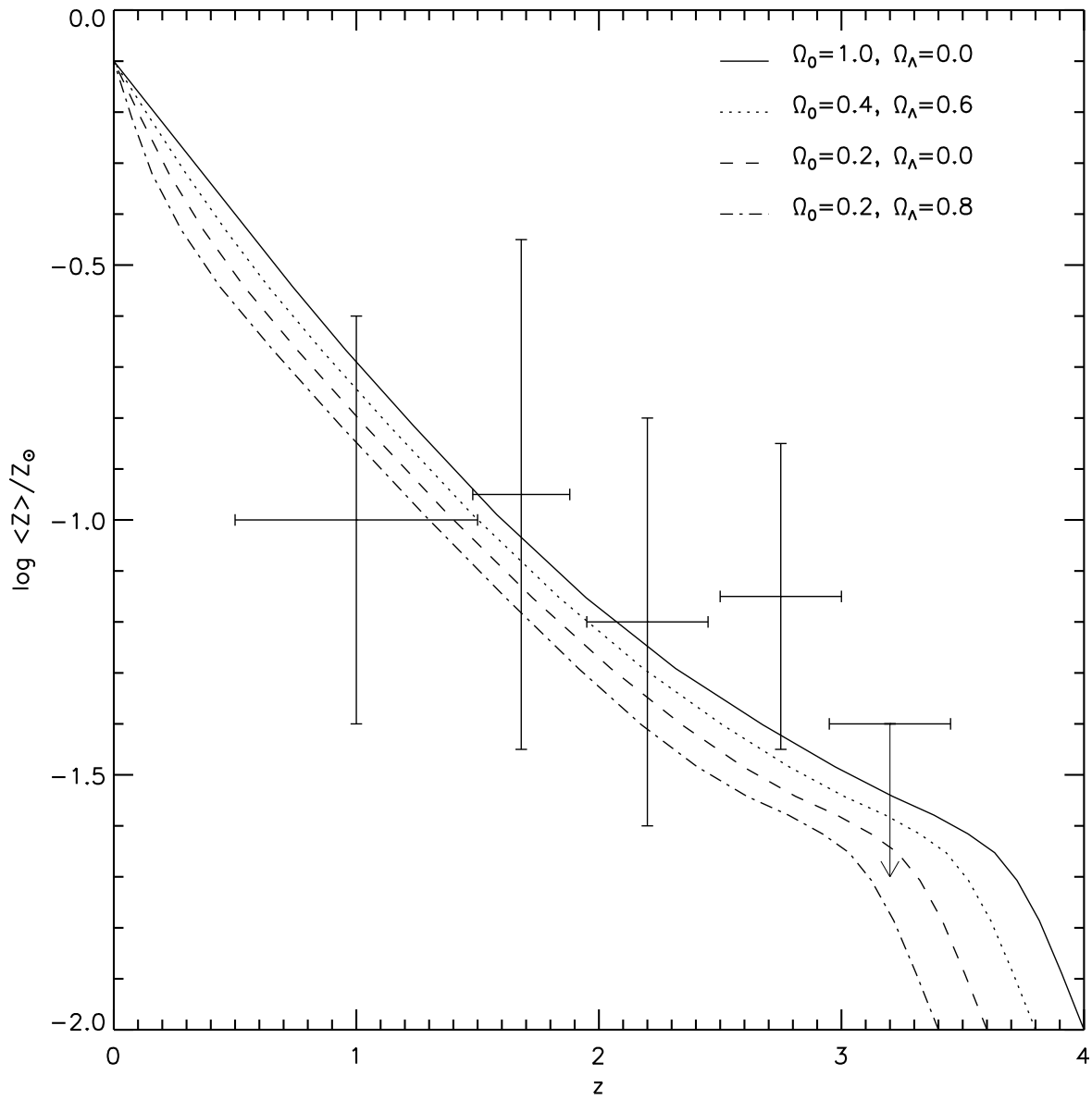


Fig. 6.—

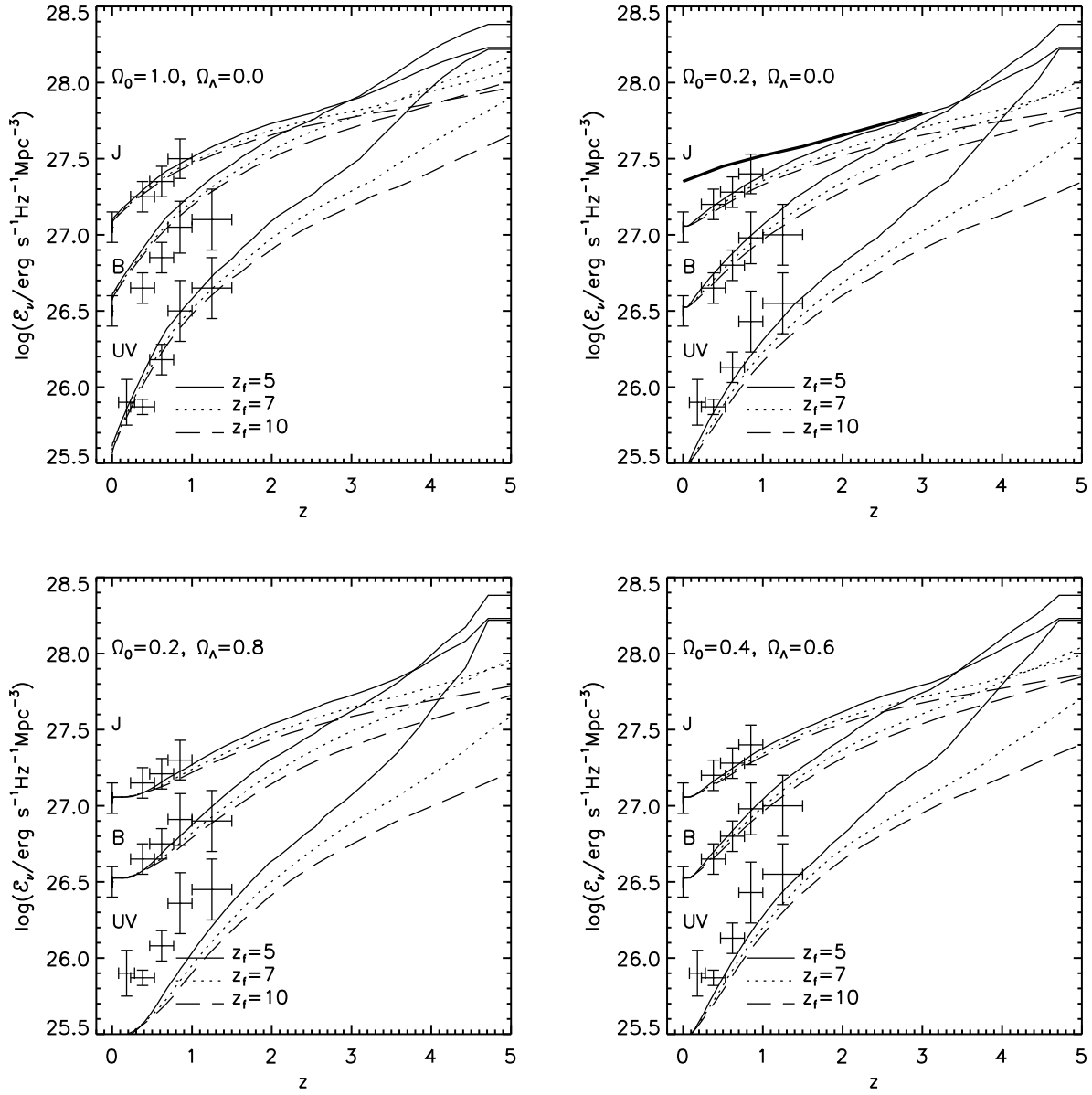


Fig. 7.—

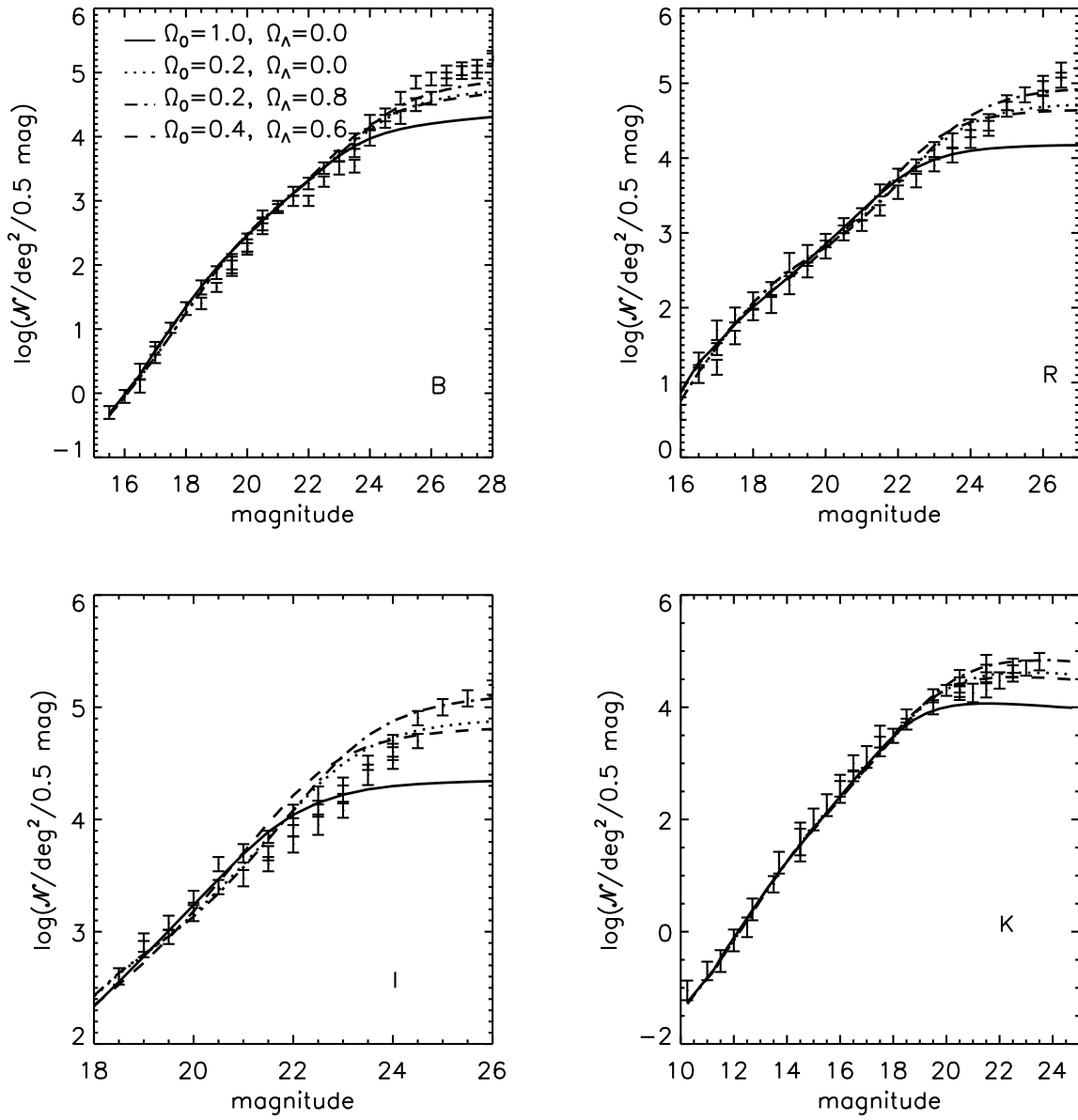


Fig. 8.—

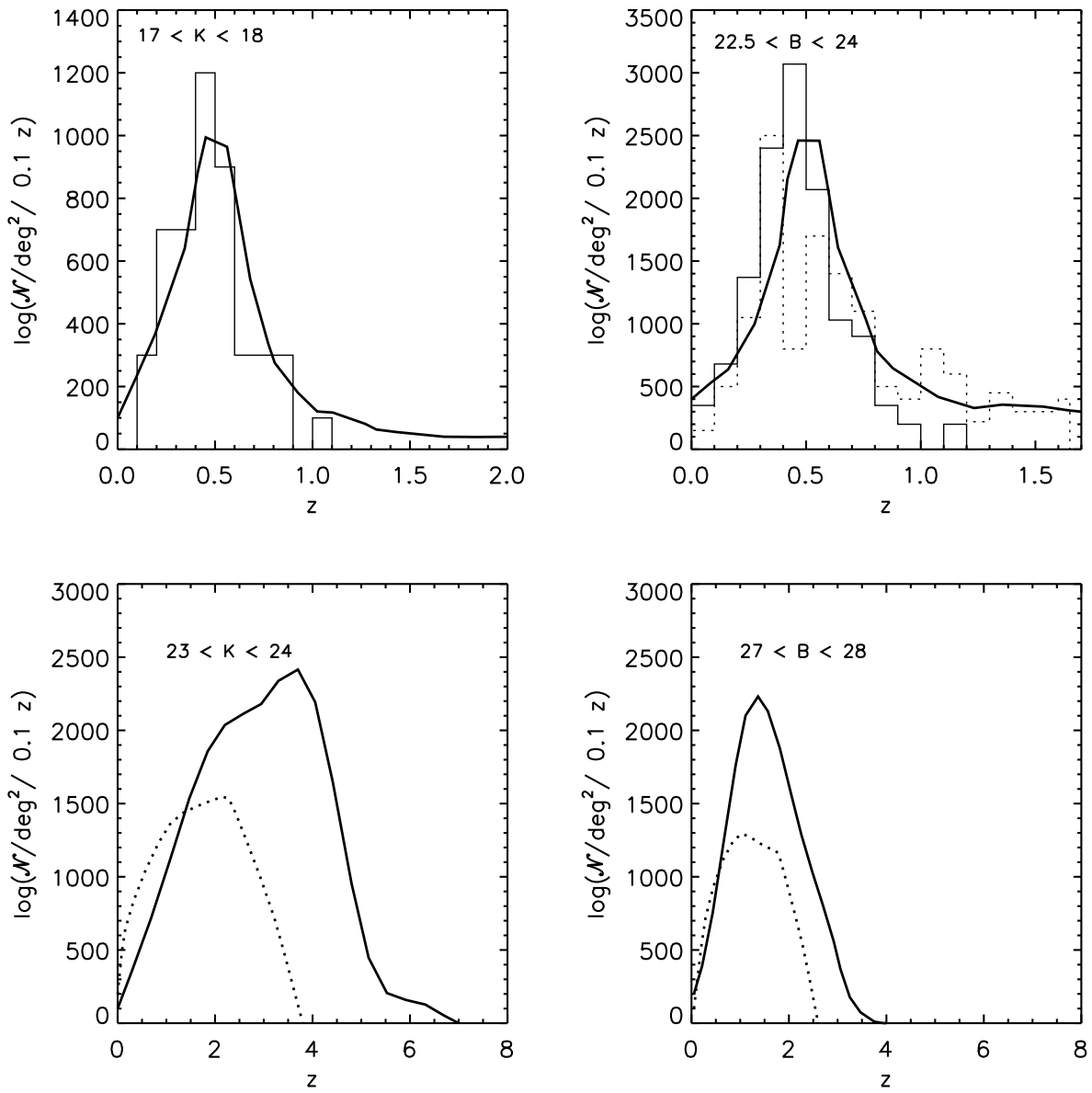


Fig. 9.—

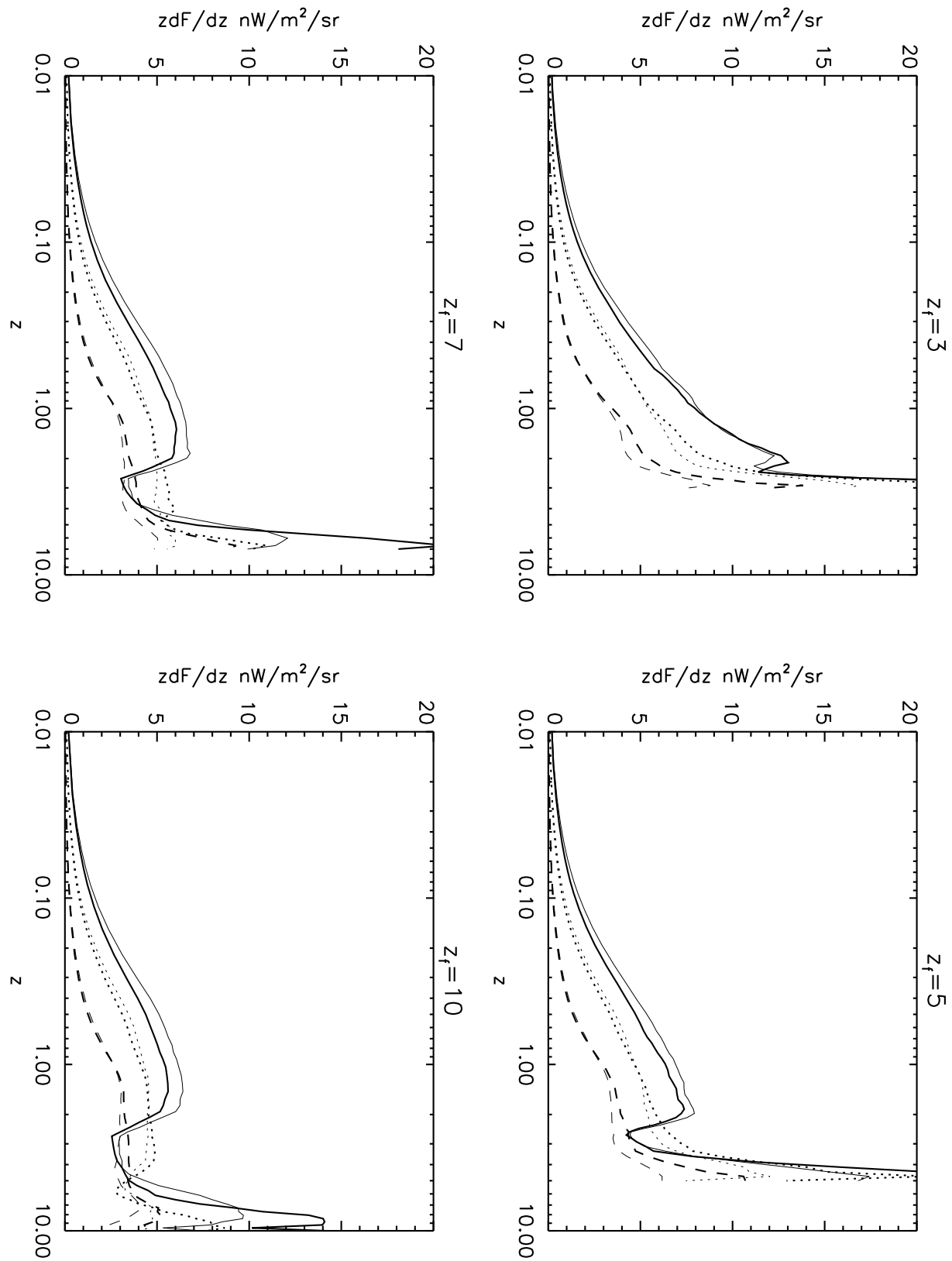


Fig. 10.—

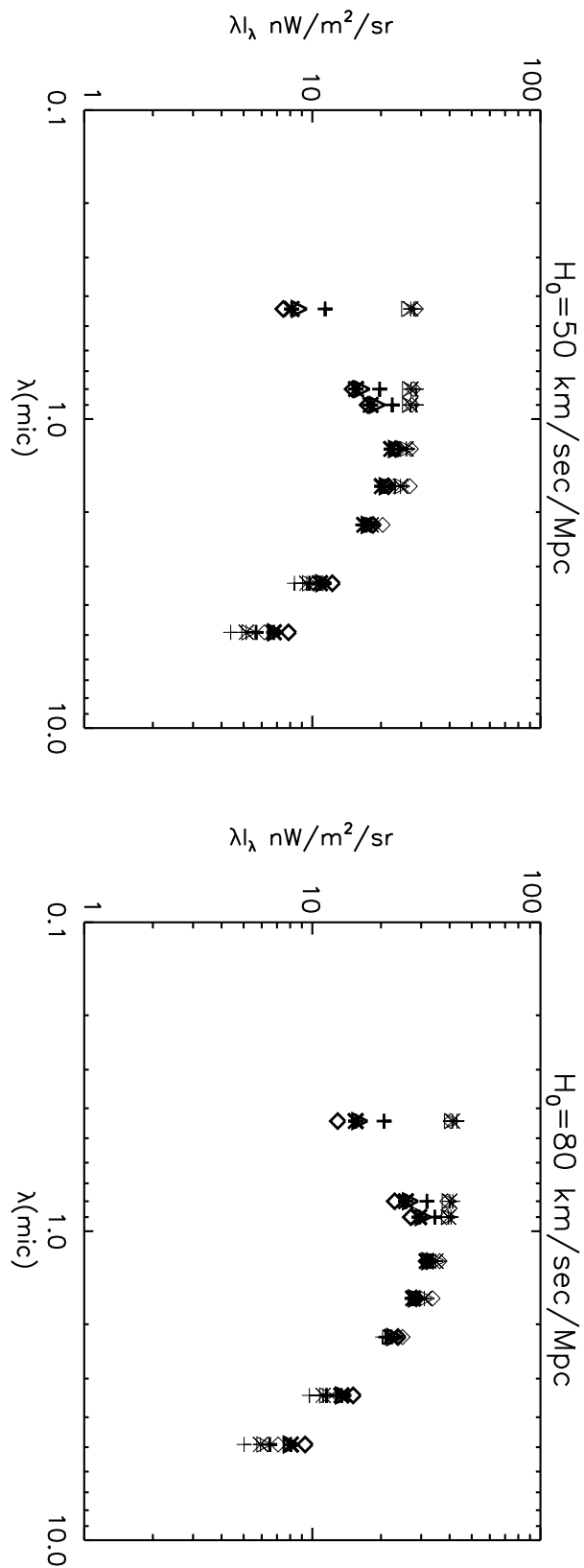


Fig. 11.—

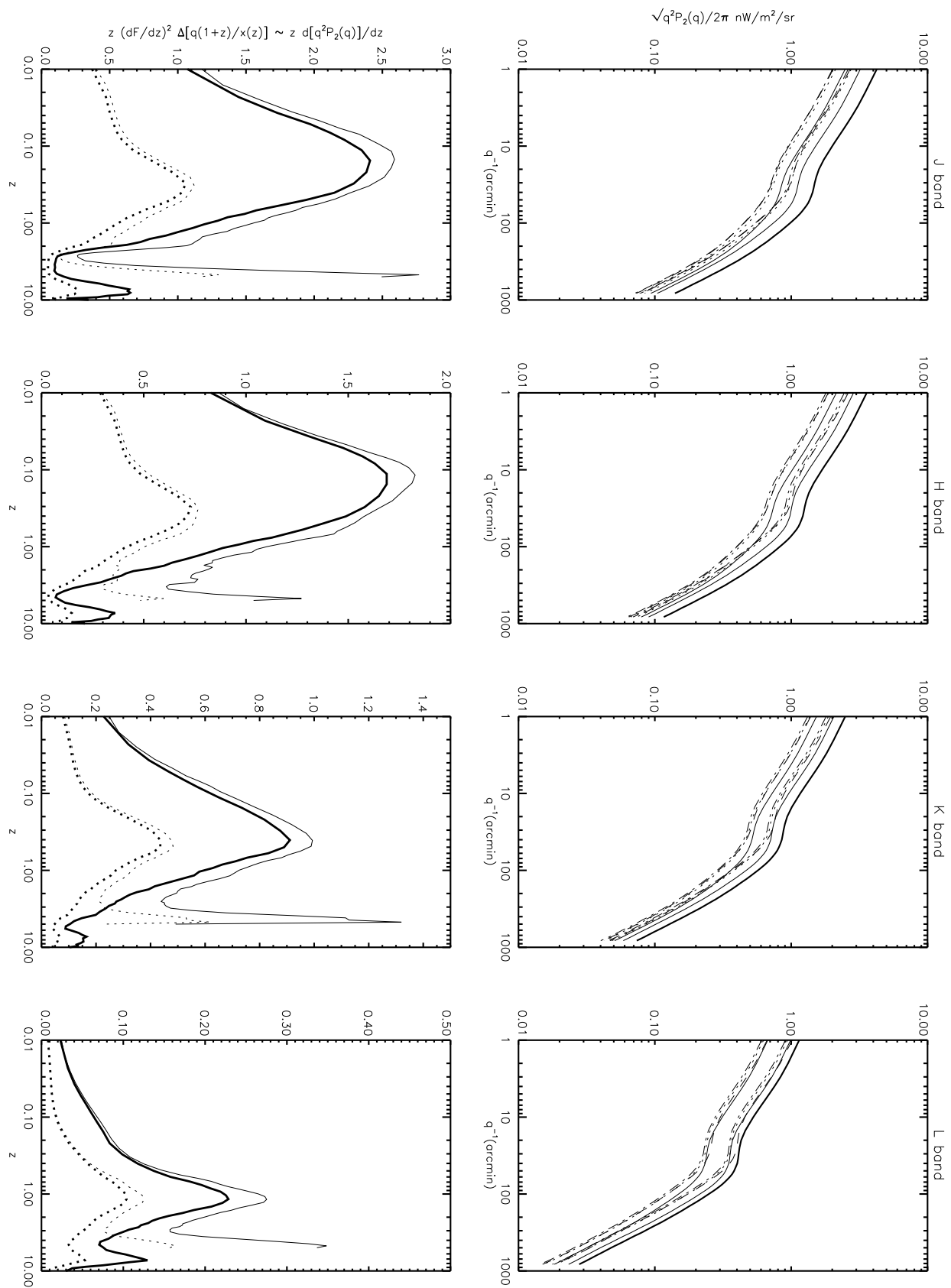


Fig. 12.—